NASA
NsG-4[illegible]

X [redacted]

THE HAYSTACK-MILLSTONE INTERFEROMETER SYSTEM

ALAN E. E. ROGERS

AD 650 838

TECHNICAL REPORT 457

MARCH 15, 1967

FACILITY FORM 602

N67-35172
(ACCESSION NUMBER)

48
(PAGES)

CR-84615
(NASA CR OR TMX OR AD NUMBER)

(THRU)
[redacted] 1
(CODE)

07
(CATEGORY)

MASSACHUSETTS INSTITUTE OF TECHNOLOGY
RESEARCH LABORATORY OF ELECTRONICS
CAMBRIDGE, MASSACHUSETTS

Acquisitioned Document
SQT

The Research Laboratory of Electronics is an interdepartmental laboratory in which faculty members and graduate students from numerous academic departments conduct research.

The research reported in this document was made possible in part by support extended the Massachusetts Institute of Technology, Research Laboratory of Electronics, by the JOINT SERVICES ELECTRONICS PROGRAMS (U.S. Army, U.S. Navy, and U.S. Air Force) under Contract No. DA 36-039-AMC-03200(E); additional support was received from the National Aeronautics and Space Administration (Grant NsG-419).

Reproduction in whole or in part is permitted for any purpose of the United States Government.

Qualified requesters may obtain copies of this report from DDC.

MASSACHUSETTS INSTITUTE OF TECHNOLOGY

RESEARCH LABORATORY OF ELECTRONICS

Technical Report 457 March 15, 1967

THE HAYSTACK-MILLSTONE INTERFEROMETER SYSTEM

Alan E. E. Rogers

(Manuscript received January 13, 1967)

Abstract

The Haystack 120-ft antenna and the Millstone 84-ft antenna have been coupled together to form a radiometric interferometer. At 18-cm wavelength, which was chosen for a study of galactic OH emission, the interferometer has a minimum fringe spacing of 54 seconds of arc. The interferometer synthesizes a beam approximately equivalent to that of a 2000-ft parabolic antenna and can measure positions to a small fraction of the fringe spacing. The interferometer uses a digital correlator to analyze the fringe amplitude and phase as a function of frequency. This enables mapping of spectral features. The design and construction are described, as well as the theory and method of data reduction. A noise analysis shows that the threshold level could be reduced by using more complex processing techniques. It is shown that for radiometric studies many of the capabilities of a very large antenna can be synthesized, with smaller antennas and complex data-processing equipment taking the place of mechanical structure.

PRECEDING PAGE BLANK NOT FILMED.

Haystack-Millstone Aerial View.

PRECEDING PAGE BLANK NOT FILMED.

TABLE OF CONTENTS

I.	INTRODUCTION	1
II.	DESIGN AND CONSTRUCTION	2
	2.1 Radio-Frequency Part of the System	2
	2.2 Intersite Coupling	2
	2.3 Digital Correlation and Data-Recording System	5
	2.4 Construction	5
	2.5 System Tests	5
III.	THEORY OF OPERATION AND METHOD OF DATA REDUCTION	9
	3.1 Geometry	9
	3.2 Computation of Spectral Fringe Amplitude and Phase	10
	3.3 Fringe Amplitude and Phase for Continuum Sources	13
	3.4 Normalized Autocorrelation Functions and Power Spectra from the Digital Correlator	14
	3.5 System Calibration	15
	3.6 Distribution of Brightness Temperature and Source Positions from Fringe Amplitude and Phase	17
	3.7 Computer Programs	19
IV.	INTERFEROMETER NOISE ANALYSIS	22
V.	POLARIZATION ANALYSIS	29
VI.	CONCLUSION	31
APPENDIX	Fortran Statement of the Program	32
Acknowledgment		40
References		41

I. INTRODUCTION

The 120-ft antenna of the Haystack Microwave Research Facility and the 84-ft antenna of the Millstone Radar Facility used as an interferometer makes a powerful instrument for high resolution radiometric studies. The antennas are separated by approximately 2250 ft along a line approximately 19° East of North. This baseline gives a minimum fringe spacing of 54 seconds of arc at 18 cm and provides a good range of projected baseline for a wide range of declination. The convenient baseline, and the spectral processing equipment at Haystack make the system ideal for a study of OH emission regions that were unresolved with a single antenna.

This report describes the design and theory of the interferometer.

II. DESIGN AND CONSTRUCTION

2.1 RADIO-FREQUENCY PART OF THE SYSTEM

A block diagram of the Millstone receiver front end is shown in Fig. 1. Circular and linear polarization is obtained from a dual-mode horn whose output ports give vertical and horizontal polarization. Combination of vertical and horizontal signals through a hybrid complex give left- and right-circular polarization after correct adjustment of the phase lengths. The antenna output is amplified by a tunnel diode amplifier and then filtered to reject the image band. A ferrite switch is included for calibration measurements. In the normal interferometer mode the switch remains switched to the antenna side. A noise source is used for single antenna measurements and system temperature measurement.

The local-oscillator signal is derived by phase-locking an oscillator to the sum or difference of a harmonic of 67 MHz and a signal whose frequency could be varied approximately 28 MHz. For the OH emission measurements the 24^{th} harmonic was selected. The output of the oscillator was filtered to attenuate any spurious signals that tend to be produced by the synchronizer. A block diagram of the local-oscillator system is shown in Fig. 2.

The mixer output is amplified by a 30-MHz amplifier with a 10-MHz bandwidth. A line driver then boosts the level to 100 Mw. The Haystack receiver front end did not require the line driver, owing to its proximity to the control room where the IF outputs are combined. Otherwise the Haystack front end is similar to that at Millstone.

2.2 INTERSITE COUPLING

The intersite coupling of the radiometers involves the transmission of antenna-pointing commands to Millstone, remote control of the radiometer, transmission of the intermediate frequency to Haystack, and two-way coupling of the local-oscillator reference signals. To maintain good phase stability, the reference signals are transmitted along a servo-controlled line that nullifies line-length changes caused by temperature change and other effects. The transmission system also has to overcome a large line attenuation of 55 db for one-way transmission at 67 MHz. The selection of a lower basic frequency would have reduced attenuation but would have made phase-locking to L-band more difficult. A block diagram of the line servo is shown in Fig. 3. The 67-MHz reference signal is amplified to approximately 1 watt and transmitted to the line through a hybrid junction. At the receiving end of the line a portion of the signal is reflected. The reflected signal undergoes phase reversal with a 100-kHz rate as the diode switch modulates the reflection coefficient from $+\frac{1}{2}$ to $-\frac{1}{2}$. Very little of the 100-kHz modulation is passed into the 67-MHz amplifier, because of the isolation afforded by the hybrid tee. At the transmitting end, the reflected signal is

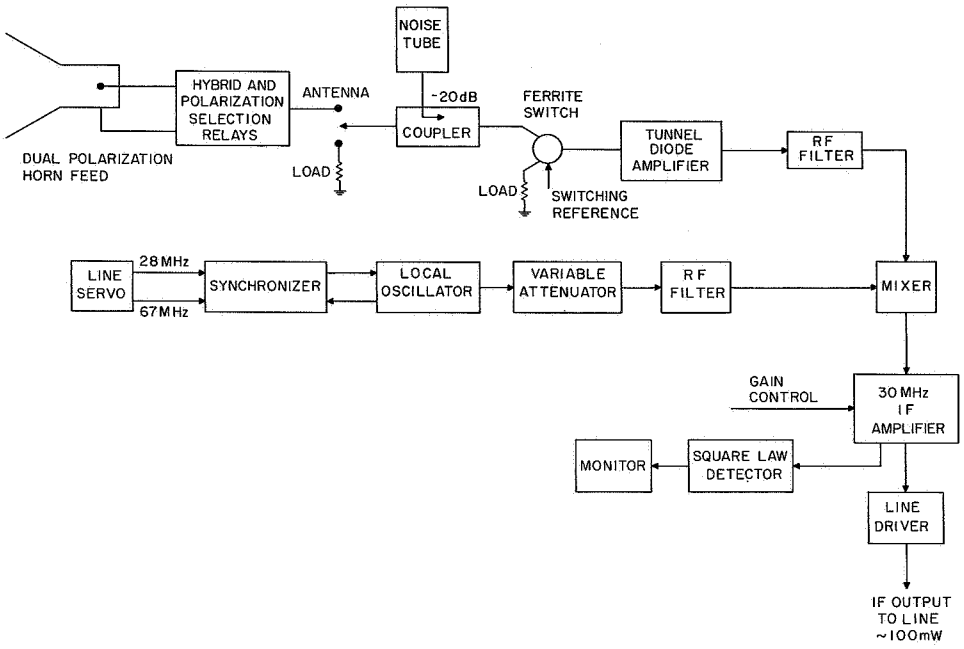


Fig. 1. Radio-frequency section of the Millstone Receiver.

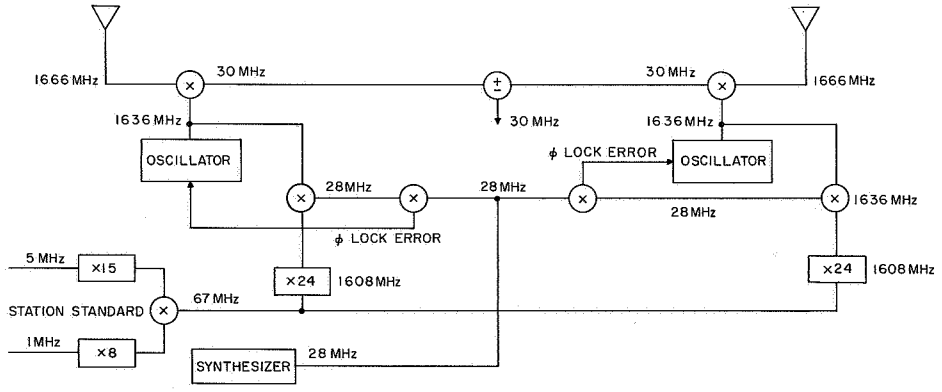


Fig. 2. Local-oscillator system shown for the center of the band at 1666 MHz.

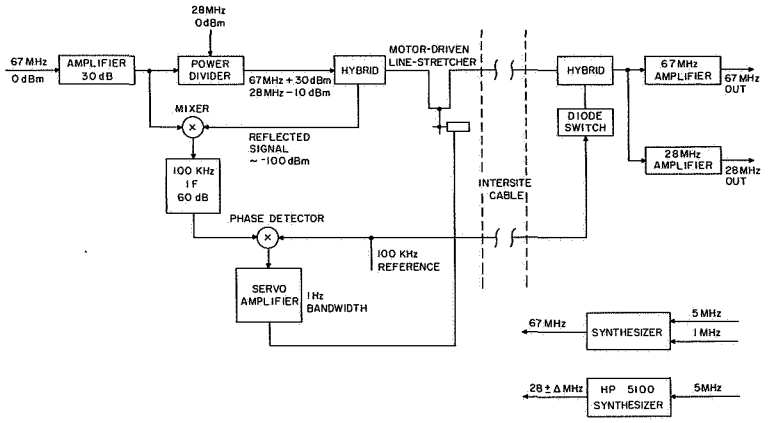


Fig. 3. Line servo to maintain phase stability.

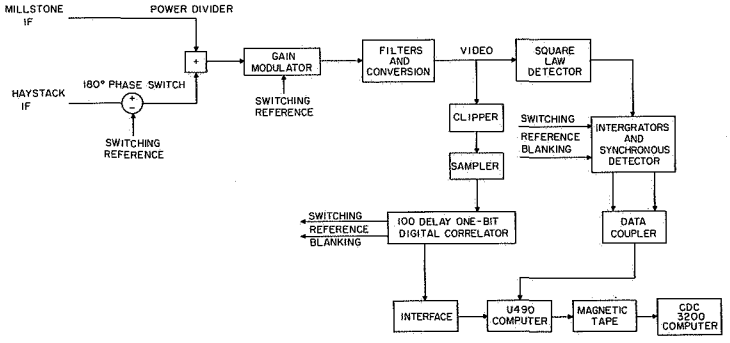


Fig. 4. Crosscorrelation scheme by addition and subtraction of IF signals.

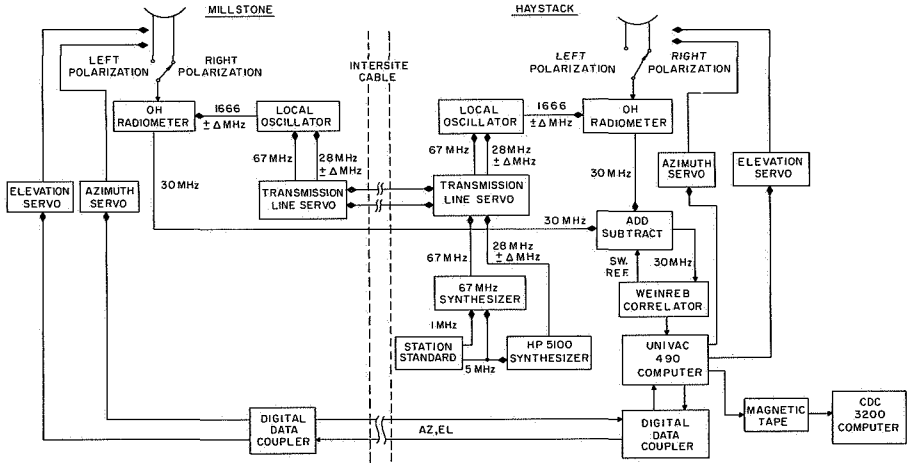


Fig. 5. Haystack-Millstone interferometer.

mixed with the 67-MHz reference signal and amplified. The output of the 100-kHz amplifier is proportional to $\cos \phi \cos 2\pi ft$, where $f = 100$ kHz, and ϕ is the phase of the 67-MHz signal after having traveled twice the line length. Multiplication of this signal by the 100-kHz reference signal produces the necessary error signal from the servo loop. The high loop gain makes it possible for the line servo to maintain a constant electrical line length to within a small fraction of an inch.

2.3 DIGITAL-CORRELATION AND DATA-RECORDING SYSTEM

The IF signals are either added or subtracted as shown in Fig. 4. The combined signal is filtered and converted to video. The autocorrelation function of the clipped and sampled video signal is taken with a digital correlator. Autocorrelation functions of the sum and difference signals are transferred alternately to a computer every 100 msec. The basic correlation period is 87.5 msec. The system is blanked for 12.5 msec while the data are being transferred to the U490 computer. Signal bandwidths of 4 MHz, 1.2 MHz, 400 kHz, 120 kHz, and 40 kHz, can be analyzed by selecting appropriate filter and sampling frequencies. The autocorrelation function is a 16-bit binary word for each of 100 delays. An extra bit is used to indicate the state of the switching reference signal. The autocorrelation functions, together with continuum data, bandwidth and correlator mode, and antenna command azimuth and elevation are transferred to magnetic tape. A block diagram of the whole system is shown in Fig. 5.

2.4 CONSTRUCTION

Figure 6 shows various sections of the interferometer equipment. The Millstone front end is located at the primary focus of the antenna, and the output of the tunnel diode amplifier is fed via a heliax cable to the equipment box on the azimuth deck. The mixer and the local-oscillator system are located in the equipment box, which is connected by the intersite cables to the radiometer box at the Haystack secondary focus. The phase combiner and digital correlator are located in the Haystack control room from which both radiometers can be controlled by remote switching.

2.5 SYSTEM TESTS

Single-antenna measurements were made to measure the aperture efficiencies. The antenna temperatures of Cassiopeia A were 160°K and 180°K, which indicated efficiencies of 40% and 25% for the Millstone and Haystack antennas, respectively. The very low efficiency for Haystack is attributed to feed losses and the flow of energy past the Cassegranian subreflector which is in the near field of the feed horn at 18 cm. The efficiency of Millstone is close to what one would expect after

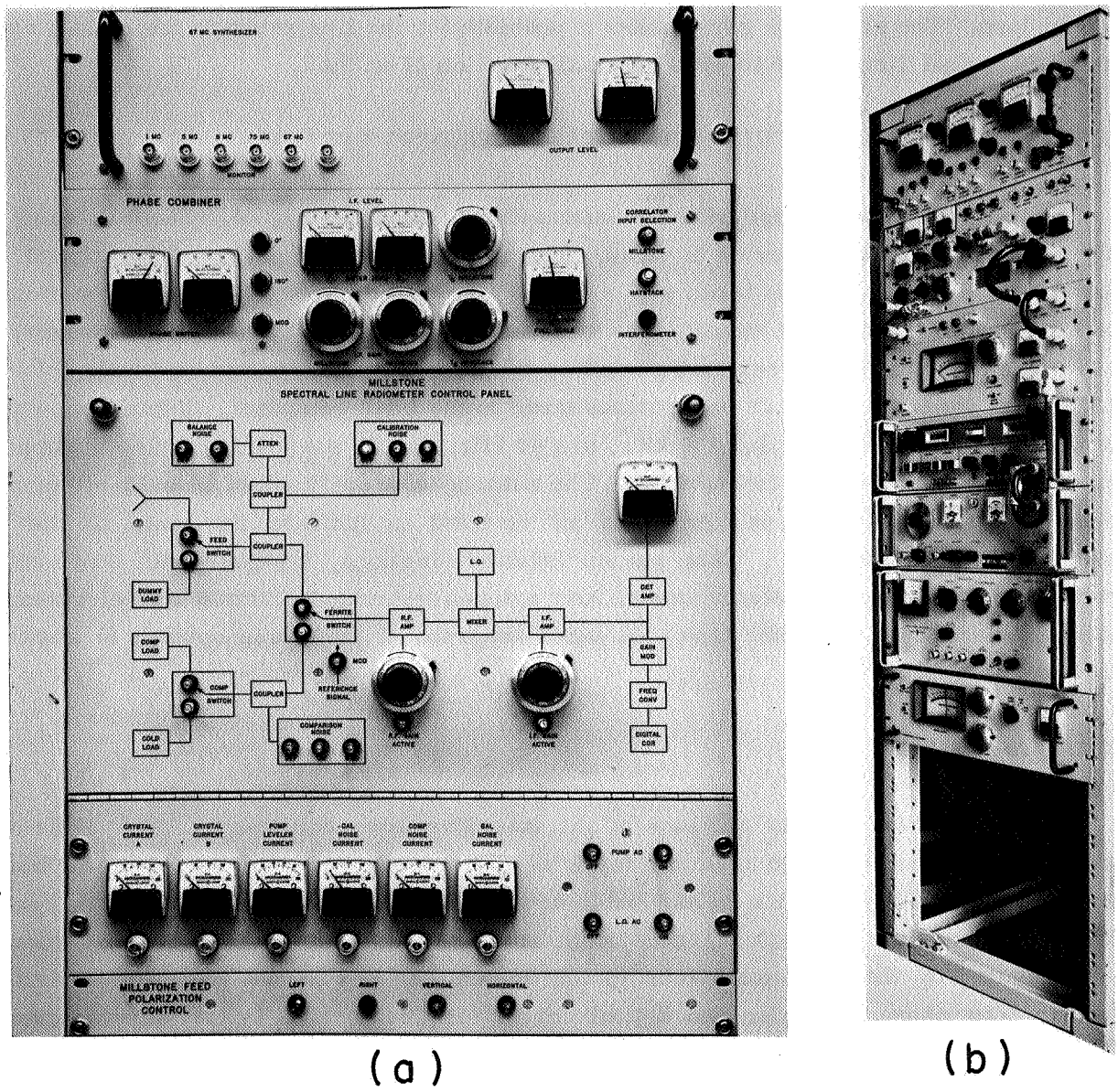
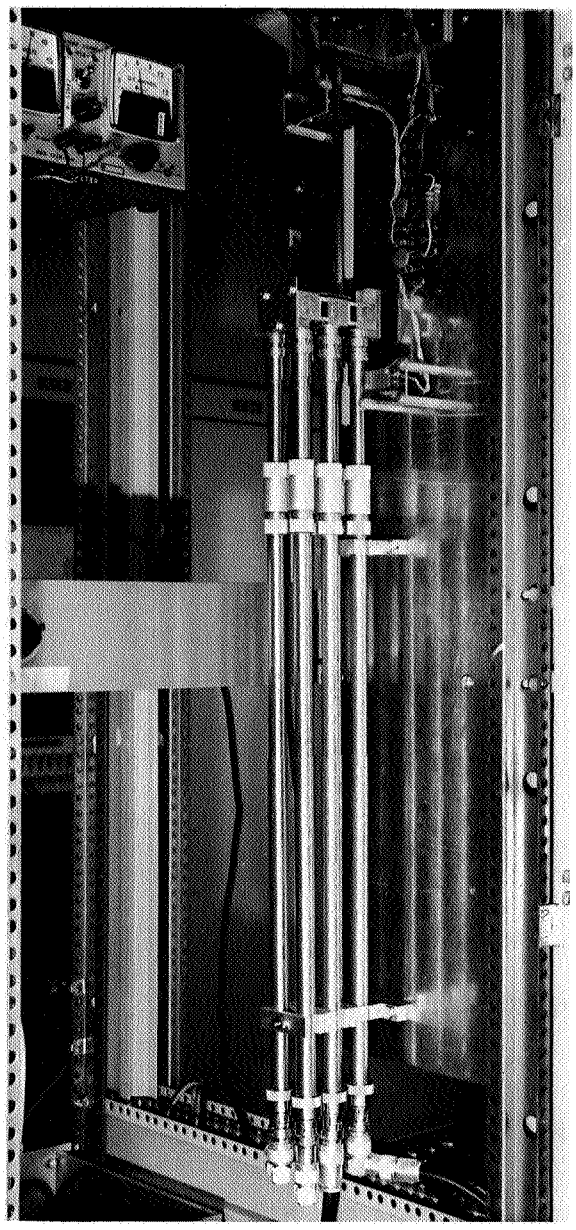
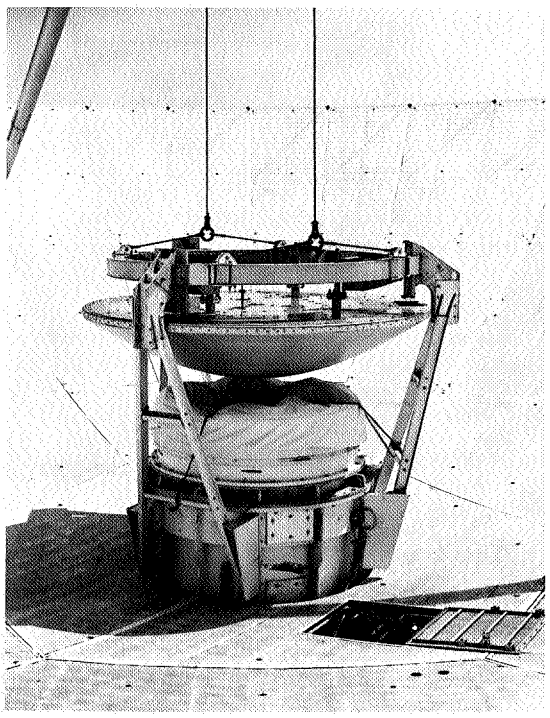


Fig. 6. (a) Control panel for the Millstone receiver.
(b) Haystack receiver rack.



(c)



(d)

Fig. 6. (c) Motor-driven line stretcher.
(d) Lowering of Millstone subreflector to make way for a prime-focus feed.

estimating the aperture blockage produced by the subreflector. For operation in the radiometric mode the Millstone subreflector was lowered to the vertex, as shown in Fig. 6d, to allow an L-band horn to be used at the primary focus.

After checking the individual radiometers for linearity, bandpass, and lack of spurious signals, the system was checked for phase coherence and phase stability. The test arrangement is illustrated in Fig. 7. A signal from a test oscillator is connected to each radiometer individually and then simultaneously. When the oscillator is swept in frequency the bandpass is displayed when only one radiometer is connected to the oscillator. When both radiometers are swept simultaneously fringes appear, because of the phase relationship between the radiometer outputs. The fringe spacing in Hz is the reciprocal of the delay in seconds. Measurement of the fringe pattern and bandpass functions showed that the phase noise in the system produced less than 2% reduction in fringe amplitudes. The phase stability was better than 50° during 24 hours. Some of this shift may have been due to the measuring technique, as observations of continuum radio sources indicated better stability.

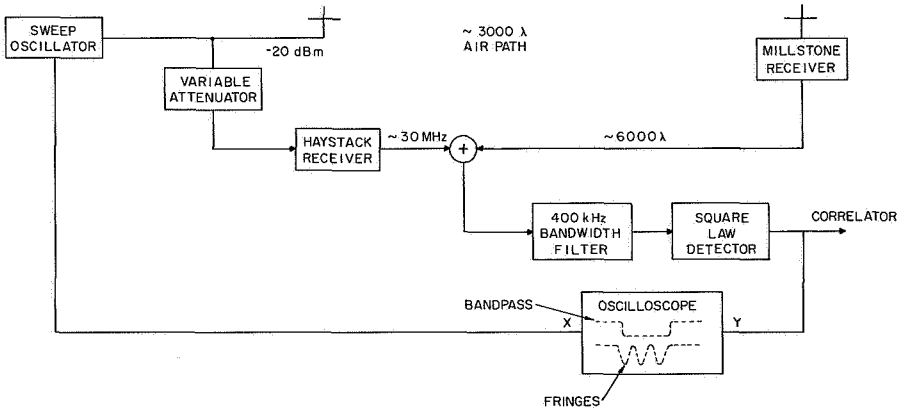


Fig. 7. Test arrangement for measuring phase coherence.

The trombone section of the line servo in Fig. 6c was observed to move approximately 5 ft during the sunrise and sunset period when the temperature changed about 50°F.

Finally, observations of unpolarized continuum radio sources with the interferometer confirmed the isolation between the two circular modes of the feeds to be better than 20 db.

III. THEORY OF OPERATION AND METHOD OF DATA REDUCTION

3.1 GEOMETRY

The interferometer geometry is shown in Fig. 8. Azimuth and elevation coordinates are centered at Haystack. $\vec{r}_1$ is a fixed vector from the intersection of the azimuth axis and a horizontal plane through the elevation axis at Millstone to the intersection of the azimuth and elevation axes of Haystack. $\vec{r}_2$ is the vector from the origin of $\vec{r}_1$ to the intersection of a line to the source through the vertex intersecting the elevation axis of Millstone; therefore, $\vec{r}_2$ is the offset of the elevation axis of Millstone from its azimuth axis. $\hat{r}_3$ is a unit vector toward the apparent position of the source. If the source position is unknown, then $\hat{r}_3$ is in the direction of a reference position in the sky relative to which the source distribution is to be mapped. These vectors may be expressed as

$$\vec{r}_1 = D \sin E_H \hat{i}_z + D \cos E_H \sin A_H \hat{i}_x + D \cos E_H \cos A_H \hat{i}_y \tag{1}$$

$$\vec{r}_2 = d \sin A_S \hat{i}_x + d \cos A_S \hat{i}_y \quad \text{(Differences in zenith neglected)} \tag{2}$$

$$\hat{r}_3 = \sin E_S \hat{i}_z + \cos E_S \sin A_S \hat{i}_x + \cos E_S \cos A_S \hat{i}_y, \tag{3}$$

where D is the distance between Haystack and Millstone, d is the offset of the elevation axis from the azimuth axis for the Millstone antenna, A_S and E_S are the apparent

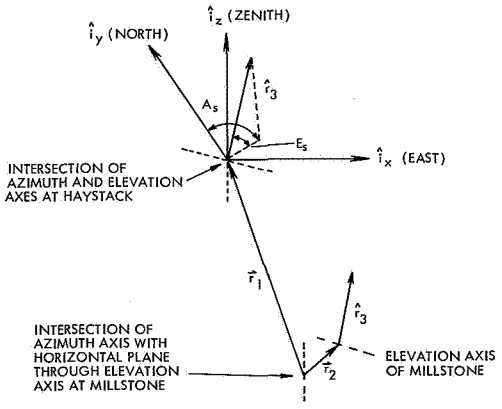


Fig. 8. Interferometer geometry.

azimuth and elevation of the source as seen from Haystack, and A_H and E_H are the azimuth and elevation of Haystack from Millstone in the Haystack coordinate system.

The portion of the interferometer delay which is azimuth- and elevation-dependent is given by

$$\tau_t = \frac{1}{c}(\vec{r}_1 - \vec{r}_2) \cdot \hat{r}_3$$

$$= \frac{D}{c} \sin E_H \sin E_S + \frac{D}{c} \cos E_H \cos E_S \cos (A_S - A_H) - \frac{d}{c} \cos E_S. \tag{4}$$

Since A_S and E_S is a function of time, so is τ_t.

3.2 COMPUTATION OF SPECTRAL FRINGE AMPLITUDE AND PHASE

The signal from a point source is a plane wave that arrives at one antenna before the other. The spectrum of the delayed signal is the same, but the frequency components in the Fourier analysis of the signal are phase-shifted. If the signals are added, the power spectrum of the added signal is modulated. This can be seen in the following way: If we let x(t) be the received signal voltage,

$$x(\omega) = \int_{-\infty}^{+\infty} x(t)\, e^{-i\omega t}\, dt, \tag{5}$$

then the Fourier transform of the delayed signal is

$$x'(\omega) = \int_{-\infty}^{+\infty} x(t-\tau_i)\, e^{-i\omega t}\, dt = e^{-i\omega\tau_i}\, x(\omega). \tag{6}$$

The power spectra of the sum and difference of the signals with and without delay are

$$S_+(\omega) = |x(\omega)|^2\, (2+2\cos\omega\tau_i) \tag{7}$$

and

$$S_-(\omega) = |x(\omega)|^2\, (2-2\cos\omega\tau_i), \tag{8}$$

where $S_+(\omega)$ and $S_-(\omega)$ are the power spectra of the added and subtracted signals, respectively. The phase that results from the interferometer delay τ_i can be expressed as the sum of component phases, according to the following equation.

$$\begin{aligned}\omega\tau_i &= (\omega_o+\Delta\omega)(\tau_t+\tau_\ell+\tau') \\ &= \omega_o\tau_t + \omega_o\tau_\ell + \Delta\omega(\tau_t+\tau_\ell) + \omega\tau',\end{aligned} \tag{9}$$

where the delay is decomposed into τ_t (as given in Eq. 4), the geometric delay for a reference position in the sky, τ_ℓ, the delay in the cables and amplifiers, and τ', the delay resulting from an offset of the point source from the reference point. The reference position is chosen to be the position toward which the main beams of the individual antennas are directed or the center of the region being mapped. $\omega_o\tau_t$ is called the reference phase, $\omega_o\tau_\ell$ the instrumental phase, and $\Delta\omega(\tau_t+\tau_\ell)$ is a frequency-dependent phase. $\omega\tau'$ is the phase developed, because of an offset of the point source from the reference phase. It is called the "fringe phase," since, in a complex source distribution, it is the phase of the Fourier component of the source distribution for the interferometer projected baseline at time t. $\frac{\omega_o}{2\pi}$ is the center of the observed band, and $\frac{\Delta\omega}{2\pi}$ is the frequency offset. $\omega\tau_t$ produces a fringe pattern in the sky, and is a function of time owing to the earth's motion.

$\Delta\omega\tau_i$ produces fringes across the spectrum or equivalently expresses the dependence of the fringe pattern on frequency. When $\Delta\omega\tau_i$ is small and there is only a fraction of a fringe over the analyzed spectrum, the interferometer is said to be in the "white fringe region." In a spectral interferometer it is only necessary to maintain the white-fringe condition over the resolution bandwidth, not the total bandwidth that is analyzed.

Thus far, only a point source has been considered. If it is assumed that different points in the sky radiate independently, then the receiver power spectrum will be just the summation of power spectra from the individual points and the difference power spectra becomes

$$S_D(\omega) = S_+(\omega) - S_-(\omega) = \sum_k |x_k(\omega)|^2 \, 4 \cos \omega\tau_i. \tag{10}$$

The only portion of $\omega\tau_i$ which changes with the summation variable, k, is $\omega\tau'_k$. Using complex quantities, we have

$$S_D(\omega) = \sum_k |x_k(\omega)|^2 \, 4 \, \mathrm{Re}\, e^{i\omega\tau_i}$$

$$= 4 \, \mathrm{Re}\, e^{i(\omega_o\tau_t + \omega_o\tau_\ell + \Delta\omega(\tau_t+\tau_\ell))} \sum_k |x_k(\omega)|^2 \, e^{i\omega\tau'_k}$$

$$= \mathrm{Re}\, A(\omega)\, e^{i\omega\tau'(\omega)}\, e^{i(\omega_o\tau_t + \omega_o\tau_\ell + \Delta\omega(\tau_t+\tau_\ell))}, \tag{11}$$

where $A(\omega)$ and $\omega\tau'(\omega)$ are known as the fringe amplitude and phase. In summing over the elementary points that make up the source distribution, the resultant phase $\omega\tau'(\omega)$ is a frequency-dependent quantity. The relation of these quantities to the brightness temperature distribution is discussed in section 3. 6.

During one integration period, typically of 10 or 15 minutes, all of the phases except the reference phase $\omega\tau_o$ remain constant to a few degrees for a source distribution contained within a few minutes of arc from the reference position. Limits for the rate of change of fringe and reference phases for the Haystack-Millstone baseline are given by

$$\frac{d\omega_o\tau_t}{dt} < 1 \text{ radian sec}^{-1}$$

$$\frac{d\omega_o\tau_\ell}{dt} \approx 0 \quad \text{(Phase-stable system)}$$

$$\frac{d\Delta\omega(\tau_t+\tau_\ell)}{dt} < \frac{\Delta\omega}{\omega_o} \text{ radians sec}^{-1}$$

$$\frac{d\omega\tau'}{dt} < 3 \times 10^{-4} \text{ radians} \quad \text{(minutes of arc displacement)}^{-1} \text{ sec}^{-1}.$$

The average fringe amplitude and phase over the integration period are determined by making a least-squares fit of the spectral difference to a function given in Eq. 11.

That is, we wish to minimize

$$\sum_t \left(S_{D,t}(\omega)-a(\omega)\cos\omega_o\tau_t-b(\omega)\sin\omega_o\tau_t\right)^2, \tag{12}$$

where

$$a(\omega) = A(\omega)\cos\left(\omega_o\tau_\ell+\Delta\omega(\tau_o+\tau_\ell)+\omega\tau'(\omega)\right) \tag{13}$$

$$b(\omega) = -A(\omega)\sin\left(\omega_o\tau_\ell+\Delta\omega(\tau_o+\tau_\ell)+\omega\tau'(\omega)\right) \tag{14}$$

$$\tau_o = \frac{\tau_t + \tau_{(t+T)}}{2} \tag{15}$$

$$T = \text{Integration period.} \tag{16}$$

$S_{D,t}(\omega)$ is the power spectrum difference for a time interval from $t - \frac{\Delta t}{2}$ to $t + \frac{\Delta t}{2}$. When the digital correlator is used, $\Delta t = 200$ msec. The reference phase change $\omega_o\left(\tau_{t+\frac{\Delta t}{2}} - \tau_{t-\frac{\Delta t}{2}}\right)$ must be small for this fringe-filtering scheme to work satisfactorily; otherwise the fringes are smeared in the difference spectrum. The addition of a frequency offset in one of the local oscillators can obviate this problem, but this was unnecessary for the Haystack-Millstone interferometer.

Minimizing the expression above, we obtain

$$\omega\tau'(\omega) = \underbrace{\tan^{-1}\left(\frac{RX(\omega) - PY(\omega)}{QX(\omega) - RY(\omega)}\right)}_{\text{with quadrant identification}} - \Delta\omega(\tau_o+\tau_\ell) - \omega_o\tau_\ell \tag{17}$$

and

$$A(\omega) = \left\{\frac{Y^2(\omega)(R^2+P^2)+X^2(\omega)(Q^2+R^2) \quad -2Y(\omega)\,X(\omega)\,R(P+Q)}{(PQ-R^2)^2}\right\}^{1/2}, \tag{18}$$

where

$$X(\omega) = \sum_t S_{D,t}(\omega)\cos\omega_o\tau_t \tag{19}$$

$$Y(\omega) = \sum_t S_{D,t}(\omega)\sin\omega_o\tau_t \tag{20}$$

$$P = \sum_t \cos^2 \omega_o \tau_t \tag{21}$$

$$Q = \sum_t \sin^2 \omega_o \tau_t \tag{22}$$

$$R = \sum_t \sin \omega_o \tau_t \cos \omega_o \tau_t. \tag{23}$$

The sine-cosine multiplications can be performed on the autocorrelation functions before taking a Fourier transform by interchanging the order of summation. In practice, this is done to save computation time.

3.3 FRINGE AMPLITUDE AND PHASE FOR CONTINUUM SOURCES

For a continuum source τ' is not a function of ω and neither is the fringe amplitude A a function of ω, provided the source spectrum is flat. Since determining spectral fringe phase and amplitude for a continuum source gives no additional information, and we would like to reduce the noise in the measurement by averaging over the bandwidth, it is desirable to modify the fringe filtering process. To do this, the least-squares fit is determined by summation over frequency in addition to time.

$$\sum_\omega \sum_t (S_{D,t}(\omega) - a \cos \omega_o \tau_t - b \sin \omega_o \tau_t)^2 = \text{minimum}. \tag{24}$$

Here we have used the following definitions:

$$a = A \cos (\omega_o \tau_\ell + \Delta\omega(\tau_o + \tau_\ell) + \omega\tau') \tag{25}$$

$$b = -A \sin (\omega_o \tau_\ell + \Delta\omega(\tau_o + \tau_\ell) + \omega\tau') \tag{26}$$

$$\omega\tau' = \tan^{-1}\left(\frac{Y_c + X_s}{Y_s - X_c}\right) - \omega_o \tau_\ell \tag{27}$$

$$A \approx \left\{ \frac{(X_s + Y_c)^2 + (Y_s - X_c)^2}{\left(\sum_\omega \sum_t \frac{1}{2}\right)^2} \right\}^{1/2}, \tag{28}$$

where

$$Y_c = \sum_\omega Y(\omega) \cos \Delta\omega(\tau_o + \tau_\ell) \tag{29}$$

$$Y_s = \sum_{\omega} Y(\omega) \sin \Delta\omega(\tau_o+\tau_\ell) \tag{30}$$

$$X_c = \sum_{\omega} X(\omega) \cos \Delta\omega(\tau_o+\tau_\ell) \tag{31}$$

$$X_s = \sum_{\omega} X(\omega) \sin \Delta\omega(\tau_o+\tau_\ell). \tag{32}$$

The exact expressions for A and $\omega\tau'$ involve a large number of terms that are very small when $\Delta\omega(\tau_o+\tau_\ell)$ undergoes a change of a few radians over the bandwidth that is analyzed. When a 1-bit correlator is used only the normalized power spectrum is obtained, so that it is impossible to obtain any fringe amplitude and phase information unless $\Delta\omega(\tau_o+\tau_\ell)$ is large enough to produce many fringes across the bandwidth.

Note that if the summation over ω is done first, then in the case of a white-fringe compensated system ($\Delta\omega(\tau_o+\tau_\ell) \ll 1$). the method is equivalent to a least-squares fit to the time-function output of an integrator preceded by a square-law detector and filter with a bandwidth of $\Delta\omega/2\pi$.

3.4 NORMALIZED AUTOCORRELATION FUNCTIONS AND POWER SPECTRA FROM THE DIGITAL CORRELATOR

A Weinreb digital autocorrelator was used to obtain the fringe amplitude and phase information from the combined IF signals.[1]

The normalized autocorrelation function $\rho(\tau)$ is obtained from the clipped-signal autocorrelation function $\rho_c(\tau)$ on the assumption of a Gaussian bivariate probability distribution for the signal[2]

$$\rho(\tau) = \sin\frac{\pi}{2}\rho_c(\tau). \tag{33}$$

The difference of normalized autocorrelation functions for the added and subtracted IF signals is given within 1% for most signals in radio astronomy by

$$D_{k,t} = \frac{(A_{k,t}-B_{k,t+100\ \mathrm{msec}})\pi}{A_{1,t}} \qquad k = 1, \ldots 100. \tag{34}$$

$A_{k,t}$ and $B_{k,t}$ (regarding positive signal as logical 1 and negative signal as logical 0) are the counter output numbers for the added a subtracted signals, respectively. The subscript k designates the delay number (1, ... 100 for the Haystack correlator). k = 1 corresponds to zero delay and consequently is just the number of samples in the integration period. This approximation to the clipping correction was made to save computer time.

The normalized difference power spectrum is obtained by taking the Fourier transform

$$S_{D,t}(i) = 2 \sum_{k=2}^{100} w_k D_{k,t} \cos\left[\frac{2\pi(i-1)(k-1)}{400}\right] \quad i = 1, \ldots 200 \tag{35}$$

$$w_k = \frac{1}{2} + \frac{1}{2}\cos\frac{\pi(k-1)}{100}, \tag{36}$$

where w_k is a cosine weighting function, and i is the frequency channel number. Usually only channels 21 to 181 are used, as these are limits where the bandpass function starts to drop. The frequency offset $\frac{\Delta\omega}{2\pi}$ is given by

$$\Delta\omega = \frac{(i-101)2\pi BW}{160}, \tag{37}$$

where BW is the bandwidth between channels 21 to 181, a quantity available to the U490 computer via the data coupler. The filter section before the correlator is designed so that channel 101 corresponds to 30.0 MHz in the IF spectrum.

The power spectrum is converted to a temperature scale by multiplying by the system temperature and dividing by the normalized power spectrum of the noise entering the clipper. This is an approximation that only holds for signal power much less than receiver noise power. The power spectrum obtained without knowledge of the signal power integrated over the bandwidth has a zero as the average value of the spectrum. The effect of this on the interferometer data is to produce an apparent fringe phase in portions of the spectrum where there is no signal. In practice, the effect is small, but it can be taken out of the data with a knowledge of the spectrum from single-antenna measurements. The exact expression for the difference spectrum in °K is given below.

$$S_{BP}(i)\, S_{D,t}(i) = S_{n,t}(i)(T_s + R_{x,t}(0)) - S_{n,t'}(i)(T_s + R_{x,t'}(0)) \tag{38}$$

$$\approx T_S(S_{n\,t'}(i) - S_{n,t'}(i)) \quad \text{for} \quad R_{x,t}(i), R_{x,t'}(i) \approx 0, \tag{39}$$

where $S_{BP}(i)$ is the bandpass function of the radiometer, $R_{x,t}(0)$ and $R_{x,t'}(0)$ are the signal temperatures at time t and t', respectively, averaged over the bandpass. $S_{n,t}(i)$ and $S_{n,t'}(i)$ are the Fourier transforms of $\sin\frac{\pi}{2}\rho_{c,t}(\tau)$, and $\frac{\pi}{2}\rho_{c,t'}(\tau)$. The approximation made to this expression only holds for continuum sources when there are many fringes across the bandwidth as we have mentioned.

3.5 SYSTEM CALIBRATION

The normalized fringe amplitude of a point source or of one that is not resolved by the interferometer is defined to be one. If it is not possible to make measurements with

zero spacing, it is necessary to calibrate the interferometer. There are two methods of calibration, both of which may be useful, the choice depending on the circumstances. The first method is to use measurements made with each antenna and radiometer individually. The individual radiometers are calibrated and the system temperatures measured. If the proportion of power from each radiometer is β, then the radiometer signals added can be written

$$\sqrt{\beta}\,\frac{\sqrt{T_{A1}}}{\sqrt{T_{S1}}}\,S_1(t) + \sqrt{\beta}\;n_1(t) + \frac{\sqrt{T_{A2}}}{\sqrt{T_{S2}}}\,S_2(t) + n_2(t), \tag{40}$$

and the subtracted signals as

$$\sqrt{\beta}\,\frac{\sqrt{T_{A1}}}{\sqrt{T_{S1}}}\,S_1(t) + \sqrt{\beta}\;n_1(t) - \frac{\sqrt{T_{A2}}}{\sqrt{T_{S2}}}\,S_2(t) - n_2(t), \tag{41}$$

where $S_1(t)$ and $S_2(t)$ are the power-normalized signal time functions, and $n_1(t)$ and $n_2(t)$ are the power-normalized receiver noise time functions. Since $n_1(t)$ and $n_2(t)$ are uncorrelated,

$$T_S = \frac{(\beta+1)}{2}\,\sqrt{T_{S1}T_{S2}}, \tag{42}$$

where T_S is the over-all system temperature, T_{S1} is the system temperature of receiver 1, T_{S2} is the system temperature of receiver 2, and

$$\beta = \frac{\text{power level from receiver 1}}{\text{power level from receiver 2}}.$$

With the system temperature defined in this manner, the fringe amplitude in °K corresponding to a normalized fringe amplitude of one (a point source) is

$$2\sqrt{\beta}\,\sqrt{T_{A1}T_{A2}}, \tag{43}$$

where T_{A1} and T_{A2} are the individual antenna temperatures. Fringe amplitudes can be normalized by dividing this expression. In order to optimize the signal-to-system temperature ratio

$$\frac{4\sqrt{\beta}}{\beta+1}\,\frac{\sqrt{T_{A1}T_{A2}}}{\sqrt{T_{S1}T_{S2}}}, \tag{44}$$

the ratio β is chosen so that $\beta = 1$, or the power levels are weighted equally. When this is done the signal-to-system temperature ratio becomes

$$\frac{2\sqrt{T_{A1}T_{A2}}}{\sqrt{T_{S1}T_{S2}}}. \tag{45}$$

The second calibration method involves no system parameters and no calibration noise sources. The procedure is to measure the power spectrum of the source from each antenna while keeping the other just off the source. Loading switching is used to make the measurement. [The phase switching may be stopped and the signals just added, since the phase switching clearly has no effect in this mode.] If the signal were originating from a point source, then the fringe amplitude would be

$$A(\omega) = \left\{\left(\sqrt{S_1(\omega)}+\sqrt{S_2(\omega)}\right)^2 - \left(\sqrt{S_1(\omega)}-\sqrt{S_2(\omega)}\right)^2\right\}$$

$$= 4\sqrt{S_1(\omega)S_2(\omega)}\,, \tag{46}$$

where $S_1(\omega)$ and $S_2(\omega)$ are the spectra from each antenna, with load switching used. Fringe amplitudes can thus be normalized by dividing by $4\sqrt{S_1(\omega)S_2(\omega)}$.

3.6 DISTRIBUTION OF BRIGHTNESS TEMPERATURE AND SOURCE POSITIONS FROM FRINGE AMPLITUDE AND PHASE

The fringe amplitude and phase provide information on the source distribution. For a general spatial distribution of incident flux, under the assumption of statistical independence of the plane waves that make up the expansion, the brightness temperature distribution and complex fringe amplitude are related by the following transform pair

$$A_{k,\ell}(\omega)\, e^{i\omega\tau'_{k,\ell}(\omega)} = \frac{2}{4\pi}\iint T_B(\omega,x,y)\, e^{ikx}\, e^{i\ell y}\sqrt{G_1(\omega,x,y)G_2(\omega,x,y)}\,dxdy \tag{47}$$

$$\iint A_{k,\ell}(\omega)\, e^{i\omega\tau'_{k,\ell}(\omega)}\, e^{-ikx}\, e^{-i\ell y}\,dkd\ell = \frac{2}{4\pi}\,4\pi^2\sqrt{G_1(\omega,x,y)G_2(\omega,x,y)}\,T_B(\omega,x,y), \tag{48}$$

where $T_B(\omega,x,y)$ is the brightness temperature at a point located at a distance x parallel to the direction of increasing Right Ascension and a distance y in Declination from the reference point. $G_1(\omega,x,y)$, $G_2(\omega,x,y)$ are the antenna gains which may be taken outside the integral, in most instances, when the region mapped with the interferometer is much smaller than the beam patterns. k and ℓ are the spatial fringe frequencies and are the coordinates of the transform or fringe-amplitude plane.

$$k = \frac{\partial\omega\tau_t}{\partial x}, \qquad \ell = \frac{\partial\omega\tau_t}{\partial y}. \tag{49}$$

A plot of the coverage of the fringe-amplitude plane for the fixed-baseline Haystack/Millstone interferometer is shown for several sources in Fig. 9.

For a fixed baseline interferometer,

$$\omega\tau_t = \frac{\omega D}{c}\left\{\sin\delta_B \sin\delta_S + \cos\delta_B \cos\delta_S \cos(L_S - L_B)\right\}, \tag{50}$$

so that

$$k = N \cos \delta_B \sin (L_S - L_B) \tag{51}$$

$$\ell = N \sin \delta_B \cos \delta_S - N \cos \delta_B \sin \delta_S \cos (L_S - L_B) \tag{52}$$

where

L_S = Hour Angle of the source

L_B = Hour Angle of the baseline

δ_S = Declination of the source

δ_B = Declination of the baseline

N = Number of wavelengths in the baseline.

The brightness temperature can be obtained by taking the Fourier transform of the fringe amplitude and phase function. Unfortunately, a fixed-baseline interferometer

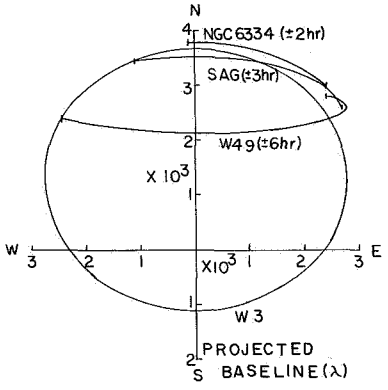


Fig. 9. Fringe-amplitude phase coverage for some OH sources. The limits shown are the observable limits.

has a very limited fringe-amplitude plane coverage, so that the transform analysis is not always used. Instead, the fringe amplitude and phase of certain model distributions are noted and compared with the observed fringe amplitude and phase. For example, the normalized fringe amplitude of a uniform disc of radius R is

$$\left| \frac{J_1\left(\frac{R}{S} 2\pi\right)}{R\pi/S} \right|,$$

where J_1 is the first-order Bessel function, and S is the fringe spacing.

$$\frac{1}{S^2} = k^2 + \ell^2. \tag{53}$$

The fringe phase for a disc is

$$\omega\tau' = \frac{D\omega}{c}\left[(\sin\delta_B \cos\delta_S)\,\Delta\delta_S + (\cos\delta_B \cos\delta_S \sin(L_S - L_B))\,\Delta R.A._S \right.$$
$$\left. - (\cos\delta_B \sin\delta_S \cos(L_S - L_B))\,\Delta\delta_S\right] \qquad (54)$$

where

$\Delta\delta_S$ = offset in Declination of center from the reference position

$\Delta R.A._S$ = offset in Right Ascension of center from the reference position

D = length of baseline.

The relations above are used to determine the position and effective source size limit when a source shows no amplitude variation with hour angle, other than that expected from the noise. The source position is determined by making a least-squares fit of the phases to an offset in position.

Other distributions that have simple fringe amplitude and phase functions are a double source which is given by vector addition of the vectors representing the complex amplitudes for the two point sources, and circularly symmetric sources which have zero phase.

3.7 COMPUTER PROGRAMS

Data processing for the Haystack-Millstone interferometer was done in two stages. First, a real-time data-processing program in the Univac-490 computer recorded autocorrelation functions on magnetic tape, together with timing and antenna pointing information, and provided a monitor on the operation of the system. The contents of this tape were then analyzed, at some later time, by a Fortran program on the CDC 3200 to derive fringe amplitude and phase.

a. Real-Time Program

For this experiment, the Haystack and Millstone antennas were controlled simultaneously by the Haystack Pointing System[3] in the Univac 490 computer. The system includes an on-line spectral-line data-processing program,[4] which was modified to allow the recording of autocorrelation functions from the digital autocorrelator at the rate of 1000 15-bit words per second. This option may be requested by the observer via the console typewriter, and does not interfere with the normal functioning of the program. Interleaved with these data records were partial system data records, which contain command pointing angles (in both celestial and horizon coordinates), computed refraction corrections, and time.

b. Fortran Fringe-Processing Program

The tape written in real time was processed by using a Fortran program. A

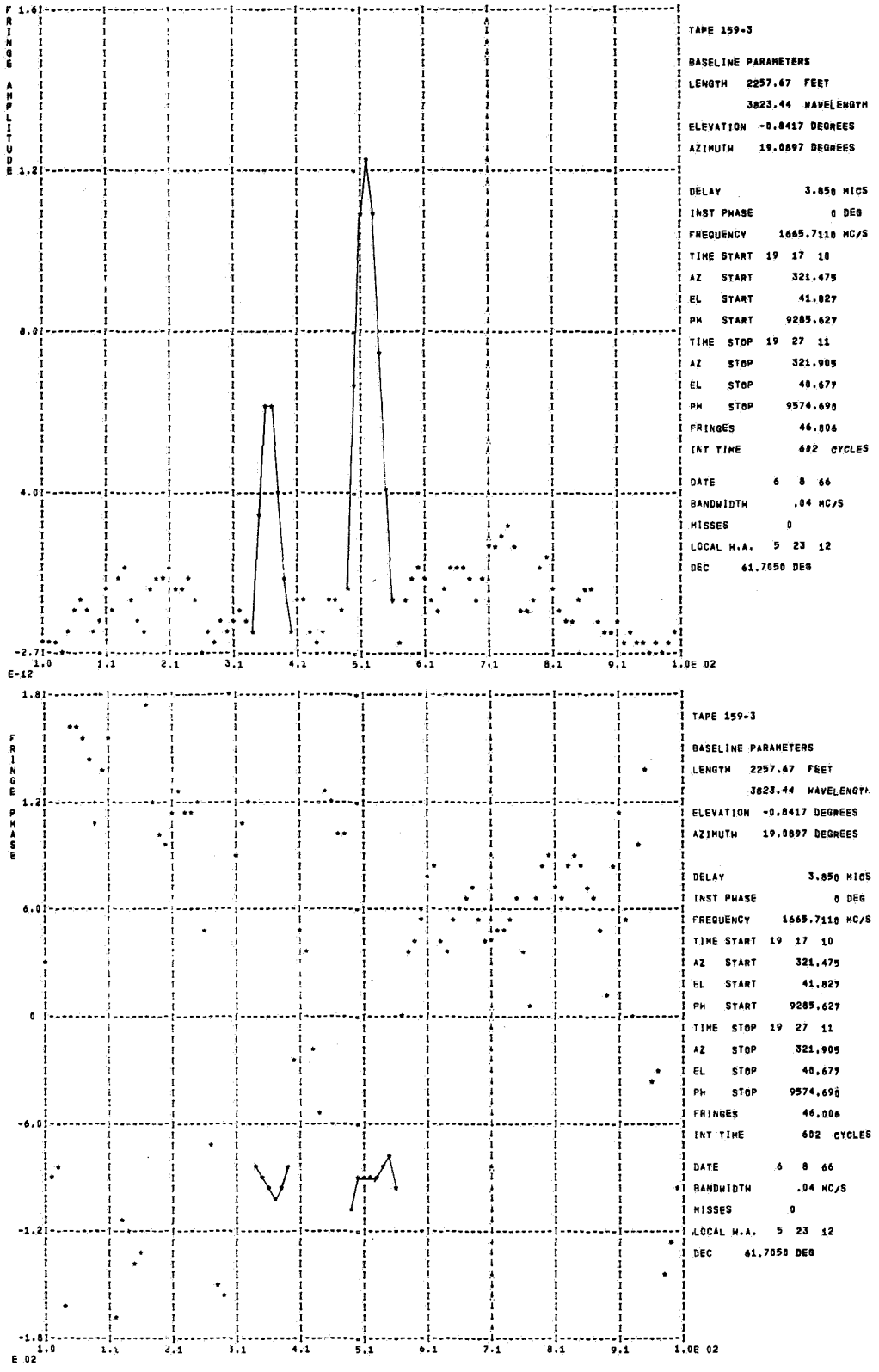


Fig. 10. High-speed printout of fringe amplitude and phase.

reference phase was computed by using the equation given in the section on interferometer geometry. The phase and amplitude were determined by the least-squares filtering technique discussed here. An example of the high-speed printout is shown in Fig. 10. The Fortran statement of the program is given in the appendix.

IV. INTERFEROMETER NOISE ANALYSIS

The difference spectrum $S_{D,t}(\omega)$ for a sample of length Δt is made up of Gaussian noise from the two receivers plus signal noise. The receiver noise waveforms are assumed to be uncorrelated, while the signal noise is correlated.

$$S_{D,t}(\omega) = A(\omega) \cos \phi(\omega) \cos \omega_o \tau_t - A(\omega) \sin \phi(\omega) \sin \omega_o \tau_t + N_t(\omega), \tag{55}$$

where

$$\phi(\omega) = \omega_o \tau_\ell + \Delta\omega(\tau_t + \tau_\ell) + \omega\tau'(\omega). \tag{56}$$

After digital filtering for a time T, during which $\cos \omega_o \tau_t$ goes through many cycles,

$$X(\omega) = PA(\omega) \cos \phi(\omega) + \sum_t N_t(\omega) \cos \omega_o \tau_t \tag{57}$$

$$Y(\omega) = -QA(\omega) \sin \phi(\omega) + \sum_t N_t \sin \omega_o \tau_t \tag{58}$$

Quantities defined in Eqs. 19-22

since $\sum_t \sin \omega_o \tau_t \cos \omega_o \tau_t \approx 0$.

The signal and noise can be represented as the sum of two vectors

$$\vec{R} = \vec{A} + \vec{N}, \tag{59}$$

where

$$\vec{A} = A(\omega) \cos \phi(\omega)\, \hat{i}_x + A(\omega) \sin \phi(\omega)\, \hat{i}y \tag{60}$$

$$\vec{N} = \frac{\sum_t N_t(\omega) \cos \omega_o \tau_t}{P} \hat{i}_x - \frac{\sum_t N_t(\omega) \sin \omega_o \tau_t}{Q} \hat{i}y \tag{61}$$

where $|\vec{R}|$ is the estimate of fringe amplitude.

The noise vector has uncorrelated components, since

$$\overline{\sum_t N_t(\omega) \cos \omega_o \tau_t \sum_t N_t(\omega) \sin \omega_o \tau_t}$$

$$= N_t^2(\omega) \sum_t \cos \omega_o \tau_t \sin \omega_o \tau_t = 0. \tag{62}$$

Assume that $\overline{N_t(\omega)\, N_{t+\Delta t}(\omega)} = 0$ and $\sum_t \cos \omega_o \tau_t \sin \omega_o \tau_t = 0$, which is a good approximation for long integration times. $N_t(\omega)$ is a Gaussian random variable so that the components of N are independent Gaussian random variables with zero means and variances, σ^2. Joint probability distribution of the components is

$$p(a_x, a_y) = \frac{1}{2\pi\sigma^2} e^{-\frac{\left(a_x^2 + a_y^2\right)}{2\sigma^2}}, \tag{63}$$

where

$$a_x = |\vec{N}| \cos\theta \tag{64}$$

$$a_y = |\vec{N}| \sin\theta \tag{65}$$

so that (see Fig. 11)

$$P\left(|\vec{N}|\right) = \frac{|\vec{N}|}{\sigma^2} e^{-\frac{|\vec{N}|^2}{2\sigma^2}} \qquad |\vec{N}| \geq 0 \tag{66}$$

$$p(\theta) = \frac{1}{2\pi} \qquad 0 \leq \theta < 2\pi \tag{67}$$

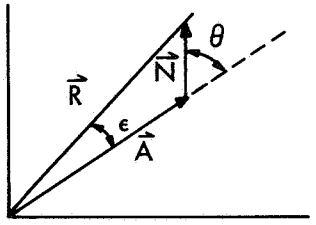


Fig. 11. Signal and noise vector.

The variance σ^2 can be computed from the variance of $N_t(\omega)$

$$\sigma^2 = \frac{\overline{\sum_t N_t^2(\omega)}\ \overline{\cos^2 \omega_o \tau_t}}{\left(\sum_t \cos^2 \omega_o \tau_t\right)^2}$$

$$= \frac{\frac{T}{\Delta t}\frac{1}{2}\overline{N_t(\omega)}}{\left(\frac{T}{\Delta t}\right)\frac{1}{4}} = \left(\frac{2\sqrt{2}\, a\, T_S}{\sqrt{T\Delta f}}\right)^2, \tag{68}$$

where Δf is the frequency resolution of the spectral measurement, (a) is a factor that normally is unity but equal to approximately 1.3 when the Weinreb correlator is used for spectral measurement. The additional factor of 2 arises from the fact that the difference spectrum is obtained by subtraction of two independent spectra, each made with integration time $\Delta t/2$.

The length of the noise vector has a Rayleigh distribution with mean

$$\overline{|\vec{N}|} = \sqrt{\frac{\pi}{2}}\,\sigma = \sqrt{\frac{\pi}{2}}\,\frac{a T_S 2\sqrt{2}}{\sqrt{\Delta f T}} \tag{69}$$

as shown in Fig. 12.

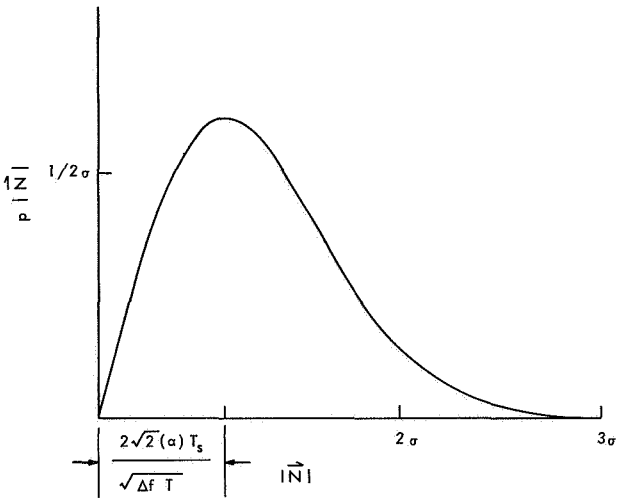


Fig. 12. Probability distribution of the amplitude of the noise vector.

The rms deviation of the amplitude and phase of the estimator is easily computed only for large signal-to-noise ratios when

$$\overline{|\vec{R}|^2} = |\vec{A}|^2 + \overline{|\vec{N}|^2} \tag{70}$$

$$\overline{|\vec{R}|} \approx |\vec{A}| \tag{71}$$

and therefore

$$\Delta R_{rms} = \left(\overline{|\vec{N}|^2}\right)^{1/2} = \sqrt{2}\ \sigma = \frac{4\alpha T_S}{\sqrt{\Delta f T}}\ ^\circ K \tag{72}$$

$$\Delta\epsilon_{rms} = \left(\frac{\overline{|\vec{N}|^2}\ \overline{\sin^2\theta}}{|\vec{A}|^2}\right)^{1/2} = \frac{\sigma}{|\vec{A}|} = \frac{2\sqrt{2}\ \alpha\ T_S}{A\sqrt{\Delta f T}}\ \text{radians}, \tag{73}$$

where A is in °K.

For any signal-to-noise ratio,

$$\Delta\epsilon_{rms} = \left\{\int_0^{2\pi}\int_0^{\infty}\left(\tan^{-1}\left(\frac{|\vec{N}|\sin\theta}{|\vec{A}| + |\vec{N}|\cos\theta}\right)\right)^2 \frac{|\vec{N}|}{\sigma^2}\, e^{-\frac{|\vec{N}|^2}{2\sigma^2}}\, d\theta d|\vec{N}|\right\}^{1/2} \tag{74}$$

which reduces to the expression above for large signal-to-noise ratios.

In practice, signals weaker than $\left(\overline{|\vec{N}|^2}\right)^{1/2}$ cannot be distinguished from the noise, and it is fairly reasonable to consider this to be the interferometer threshold. Figure 9, showing a plot of fringe spectral amplitude and phase, clearly illustrates the significance of the threshold.

The interferometer threshold can be reduced by using other schemes of processing. It will be shown that the system used here is a factor of 2 from optimum. The antenna signals for a point source can be considered for the purpose of this discussion. Signals from a more complex source are assumed to be the sum of uncorrelated components. The output of the two receivers can be written

$$x(t) = \sqrt{\tilde{T}_{A_1}}\, S(t) + \sqrt{T_{S_1}}\, n_1(t) \tag{75}$$

$$y(t) = \sqrt{\tilde{T}_{A_2}}\, S(t+\phi) + \sqrt{T_{S_2}}\, n_2(t), \tag{76}$$

where the function ϕ is assumed to remain constant during the correlation time Δt. The spectrum of the receiver noise is assumed to be unity over the bandwidth considered. Spectral information is contained in the autocorrelation functions

$$\int_{-t'}^{t'} \langle x(t)x(t-\tau)\rangle\, e^{-i\omega\tau}\, d\tau = \tilde{T}_{A_1} S(\omega) + T_{S_1} + T_{S_1} S_{n_1}(\omega), \tag{77}$$

where $S_{n_1}(\omega)$ is the noise in the measurement. The angular brackets denote time averaging over the integration period. Cross terms are omitted, under the assumption that the signal power is much less than the receiver noise.

$$\overline{S_{n_1}(\omega)} = 0 \tag{78}$$

$$\overline{S^2_{n_1}(\omega)} = \frac{1}{\Delta f \Delta t}, \tag{79}$$

where Δf is the spectral resolution, and $\overline{S^2_{n_1}(\omega)}$ is the variance of spectral measurement derived under the assumption of Gaussian statistics for the noise. The information about ϕ is contained in the crosscorrelation function,

$$2\int_{-t'}^{t'} \langle x(t)y(t-\tau)\rangle\, e^{-i\omega\tau}\, d\tau = 2\sqrt{\tilde{T}_{A_1}\tilde{T}_{A_2}}\, e^{-i\omega\phi}\, S(\omega)$$

$$+ 2\sqrt{T_{S_1}T_{S_2}}\, (\mathrm{Re}\, S_n(\omega) + i\, \mathrm{Im}\, S_n(\omega)), \tag{80}$$

where the real and imaginary parts of the cross spectral function $S_n(\omega)$ will be shown to be independent noise terms. The factor of 2 is introduced to make the signal equal to $2\sqrt{\tilde{T}_{A_1}\tilde{T}_{A_2}}$. $\tilde{T}_{A_1}$ and $\tilde{T}_{A_2}$ are the average antenna temperatures over the bandwidth considered. That is,

$$\int_{-\infty}^{+\infty} T_A(\omega)\, \frac{d\omega}{2\pi} = \int_{-\infty}^{+\infty} \tilde{T}_A S(\omega)\, \frac{d\omega}{2\pi} = \tilde{T}_A. \tag{81}$$

The independence of Re $S_n(\omega)$ and Im $S_n(\omega)$ can be proved by showing them to be uncorrelated.

$$\overline{\text{Re } S_n(\omega) \text{ Im } S_n(\omega)} = \iint \overline{\langle n_1(t)n_2(t-\tau)\rangle \langle n_1(t')n_2(t'-\tau')\rangle} \sin\omega\tau \cos\omega\tau' \, d\tau d\tau'$$

$$= \iint \overline{\langle n_1(t)n_1(t')\rangle \langle n_2(t-\tau)n_2(t'-\tau')\rangle} \sin\omega\tau \cos\omega\tau' \, d\tau d\tau'$$

$$= 0. \tag{82}$$

To find the variance of Re $S_n(\omega)$ and Im $S_n(\omega)$, consider the variance of the terms in the spectrum of added noise

$$\int_{-t'}^{t'} \langle (n_1(t)+n_2(t)\rangle \langle (n_1(t-\tau)+n_2(t-\tau)\rangle \, e^{-i\omega\tau} \, d\tau$$

$$= S_{n_1}(\omega) + S_{n_2}(\omega) + \text{Re } S_n(\omega) + i \text{ Im } S_n(\omega) + \text{Re } S_n(\omega) - i \text{ Im } S_n(\omega). \tag{83}$$

The variance of the spectral estimate for the added signal is $\frac{4}{\Delta f \Delta t}$ because adding the uncorrelated Gaussian signals gives a Gaussian signal with twice the power. Thus

$$\text{Var}\left[S_{n_1}(\omega)+S_{n_2}(\omega)+2 \text{ Re } S_n(\omega) \right] = \frac{4}{\Delta f \Delta t}. \tag{84}$$

The individual terms are independent. Clearly, $S_{n_1}(\omega)$ and $S_{n_2}(\omega)$ are independent. $S_{n_1}(\omega)$ and Re $S_n(\omega)$ can be shown to be independent in the following manner.

$$\overline{\text{Re } S_n(\omega) S_{n_1}(\omega)} = \iint \overline{\langle n_1(t)n_1(t-\tau)\rangle \langle n_1(t')n_2(t'-\tau')\rangle} \cos\omega\tau \cos\omega\tau' \, d\tau d\tau'$$

$$= \iint \Big(\overline{\langle n_1(t)n_1(t-\tau)\rangle} \; \overline{\langle n_1(t')n_2(t'-\tau')\rangle}$$

$$+ \overline{\langle n_1(t)n_1(t')\rangle} \; \overline{\langle n_1(t-\tau)n_2(t'-\tau')\rangle}$$

$$+ \overline{\langle n_1(t)n_2(t'-\tau')\rangle} \; \overline{\langle n_1(t-\tau)n_2(t')\rangle} \Big) \quad \cos\omega\tau \cos\omega\tau' \, d\tau d\tau'$$

$$= 0, \tag{85}$$

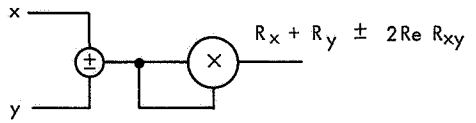
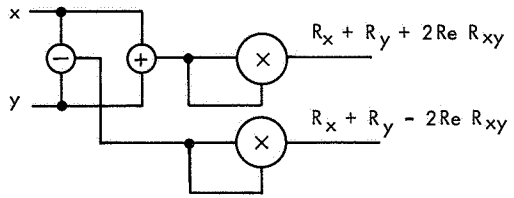
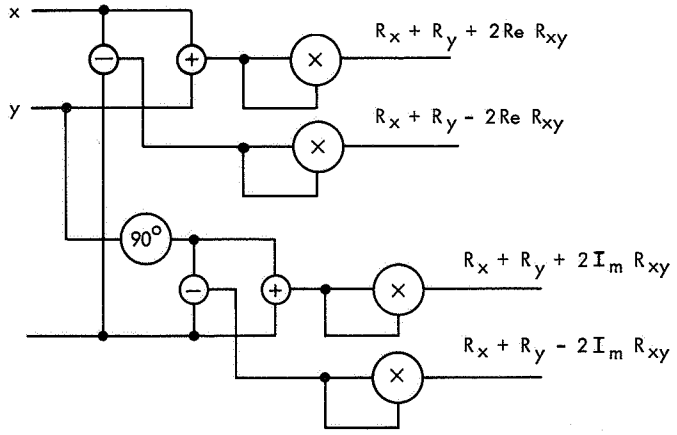
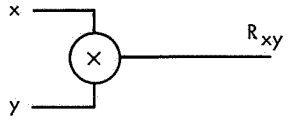
since n_1 and n_2 are independent. Therefore

$$\text{Var}\left[S_{n_1}(\omega) + S_{n_2}(\omega) + 2 \text{ Re } S_n(\omega) \right] = \text{Var } S_{n_1}(\omega) + \text{Var } S_{n_2}(\omega) + \text{Var } 2 \text{ Re } S_n(\omega), \tag{86}$$

so that

$$\text{Var Re } S_n(\omega) = \frac{1}{2\Delta f \Delta t}. \tag{87}$$

Table 1. Interferometer detection schemes and noise thresholds.

Interferometer Radiometer Type	Schematic	Noise Threshold $\left(\overline{N^2}\right)^{1/2}$	Comments
1. Add-Subtract Autocorrelation		$\frac{4\,T_s}{\sqrt{\Delta f\, T}}$	$T_s = \sqrt{T_{s_1} T_{s_2}}$ If signal powers are added equally
2. Simultaneous Add-Subtract Autocorrelation		$\frac{2\sqrt{2}\;\; T_s}{\sqrt{\Delta f\, T}}$	In schemes 1 and 2 for fringe reduction least squares fit is used and source motion required
3. Simultaneous Add-Subtract Autocorrelation with Quadrature		$\frac{2\,T_s}{\sqrt{\Delta f\, T}}$	Optimum system if signals added in correct ratio to minimize T_s
4. Crosscorrelation		$\frac{2\,T_s}{\sqrt{\Delta f\, T}}$	Optimum System . Fringe reduction does not require source motion $T_s = \sqrt{T_{s_1} T_{s_2}}$

The variance of Im $S_n(\omega)$ is the same as the variance of Re $S_n(\omega)$. This can be shown by introducing 90° phase shift in x or y. Then

$$2\int_{-t'}^{t'} \left\langle x(t+a)y(t-\tau)\right\rangle \; e^{-i\omega\tau}\, d\tau = 2\int_{-t'}^{t'} \left\langle x(t)y(t-\tau')\right\rangle \; e^{i\omega a}\, e^{-i\omega\tau'}\, d\tau'$$

$$= 2i\, e^{-i\omega\phi} \sqrt{\tilde{T}_{A_1}\tilde{T}_{A_2}}\, S(\omega) + 2\sqrt{T_{S_1}T_{S_2}}\,(-\mathrm{Im}\, S_n(\omega) + i\,\mathrm{Re}\, S_n(\omega)). \qquad (88)$$

If the crosscorrelation technique were applied to the signal from one antenna it would have an rms of $\sqrt{2}$ times the rms for a total power radiometer. This is seen by setting $\phi = 0$, and considering only the real part of the transform. The signal is T_A, and the rms noise $\frac{T_S\sqrt{2}}{\sqrt{\Delta f \Delta t}}$. The factor of two is dropped for the signal, because of the 3 db lost in the division of power to the two receivers. When crosscorrelation is used to determine ϕ and $S(\omega)$, the signal vector is $2\sqrt{\tilde{T}_{A_1}\tilde{T}_{A_2}}\, S(\omega)\, e^{-i\omega\phi}$ and the noise vector, which has components $2\sqrt{\tilde{T}_{S_1}\tilde{T}_{S_2}}\,\mathrm{Re}\, S_n(\omega)$ and $2\sqrt{T_{S_1}T_{S_2}}\,\mathrm{Im}\, S_n(\omega)$, each with variance $\frac{2}{\Delta f \Delta t}$, thus has an rms deviation of $\frac{\sqrt{2}\,\sqrt{2}\,\sqrt{T_{S_1}T_{S_2}}}{\sqrt{\Delta f \Delta t}}$ (from Eq. 72). The averaging or filtering of the crosscorrelation functions to take out the time-variant component (resulting from the earth's rotation) of ϕ is accomplished by multiplying by $e^{\omega\tau_t}$ and summing. This is equivalent to the least-squares fit technique, but is much simpler, owing to the existence of the imaginary component.

The crosscorrelation function contains all the fringe information and the best estimate of this function must be the optimum system. It might be questioned whether it is the optimum scheme when it is clear that even if we know the fringe phase in advance of the source position and want to estimate the source flux, the system has $\sqrt{2}$ more noise than a total power radiometer which is known to be optimum. If measurements of flux are to be made, however, with a total power radiometer, half the observing time should be spent determining the receiver noise power. The increase of $\sqrt{2}$ in the noise of the crosscorrelation estimate is offset by the added information (receiver noise has been subtracted out) in the crosscorrelation function. Table 1 shows various interferometer detection schemes and their noise thresholds. One disadvantage of crosscorrelation should be noted. The spectral resolution obtainable with a crosscorrelator is half that of an autocorrelator with the same number of delays. The reason is that crosscorrelation functions are not symmetric, and require both positive and negative delays to extract the available information.

V. POLARIZATION ANALYSIS

An interferometer can be used to analyze the polarization of a radio source. A complete set of polarizations can be obtained from the autocorrelation functions of two orthogonal polarizations plus the complex crosscorrelation function between the two polarizations. For right, left, and two sets of linear equations, we have

$$2S_R(\omega) = S_H(\omega) + S_V(\omega) + 2 \text{ Im } S_{H,V}(\omega) \tag{89}$$

$$2S_L(\omega) = S_H(\omega) + S_V(\omega) - 2 \text{ Im } S_{H,V}(\omega) \tag{90}$$

$$2S_{45°}(\omega) = S_H(\omega) + S_V(\omega) + 2 \text{ Re } S_{H,V}(\omega) \tag{91}$$

$$2S_{-45°}(\omega) = S_H(\omega) + S_V(\omega) - 2 \text{ Re } S_{H,V}(\omega) \tag{92}$$

where

$$S(\omega) = \int_{-\infty}^{+\infty} R(\tau)\, e^{-i\omega\tau}\, d\tau. \tag{93}$$

These relations are derived from the autocorrelation functions. For example,

$$\sqrt{2}\, x_R(t) = x_H(t) + x_V(t+90°); \tag{94}$$

therefore,

$$2R_{x_R}(\tau) = R_{x_H}(\tau) + R_{x_V}(\tau) + R_{x_H x_V}(\tau-90°) + R_{x_H x_V}(-\tau-90°) \tag{95}$$

and hence

$$2S_R(\omega) = S_H(\omega) + S_V(\omega) + 2 \text{ Im } S_{H,V}(\omega). \tag{96}$$

When both elements of the interferometer have the same polarization, the autocorrelation function is measured. For example,

$$\int_{-\infty}^{+\infty} R_{x_V}(\tau-\phi)\, e^{-i\omega\tau}\, d\tau = e^{-i\omega\phi}\, S_V(\omega). \tag{97}$$

When the interferometer is used with elements having orthogonal polarizations the crosscorrelation function is obtained but real and imaginary parts of the Fourier transform can only be separated from the fringe phase information by making measurements with polarizations exchanged.

$$\int_{-\infty}^{+\infty} R_{x_H x_V}(\tau-\phi)\, e^{-i\omega\tau}\, d\tau = e^{-i\omega\phi}\ \{\text{Re } S_{H,V}(\omega) + i \text{ Im } S_{H,V}(\omega)\}, \tag{98}$$

while

$$\int_{-\infty}^{+\infty} R_{x_V x_H}(\tau-\phi)\, e^{-i\omega\tau}\, d\tau = e^{-i\omega\phi}\ \{\text{Re } S_{H,V}(\omega) - i \text{ Im } S_{H,V}(\omega)\}. \tag{99}$$

For an extended source, both of these measurements are required to obtain the polarization parameters over the source distribution. With the use of vertical and horizontal polarizations as an example, the Fourier transform of the fringe amplitude for vertical polarization yields the distribution of vertical polarization, and similarly for the horizontal polarization, while the distribution of right minus left and +45° polarization minus −45° polarization are given by the transform of the sum and difference of complex amplitudes made with one element of the interferometer vertical and the other horizontal, and vice versa.

VI. CONCLUSION

This report shows that while a digital correlator (with phase switching), or a digital crosscorrelator, is useful for a spectral interferometer it also has many advantages when spectral information is not required. It is interesting to note that the optimum receiver system for making a radiometric map as a function of frequency and polarization, with two single-feed antennas used, consists of 4 receivers and 4 crosscorrelators: one receiver on each of the two orthogonal polarization ports of each antenna, and the crosscorrelators between pairs of receivers, one on each antenna.

APPENDIX

Fortran Statement of the Program

```
                                    3200  FORTRAN    (2.1)

      PROGRAM MILSTAK
      DIMENSION CT(400),WK(100),F(2418),T(2418),ASUM(200),SC(3108),
     1 PAR(238),NH(102) ,ISUM(2,100,5),AZS(6),TIME(6),ELS(6),PH(6),
     2          PHREF(5),X(100),Y(100),XT(200),YT(200),PHASE(200),
     3 AMP(200),CPR(5),SPR(5),TITLE(21),PA(80),ANS(10),PHA(200),
     4 LABELX(6),LABELY(8), KI(4),TIT(21),
     5 INFO(364),PNH(102),U(100),Z(100),TRANS(200),NHT(28),CP(5),SP(5)
      COMMON ISUM,S,D,PHA,PHASE
      CHARACTER PA,PNH
      EQUIVALENCE (NH,PNH)
      INTEGER TITLE,REPLY,TIT,OT
      PIE=3.1415926536
      R=3.141592653/180.
      READ 1,DMIL,DBAS,ELB,AZB
    1 FORMAT(4F10.4)
      CEB=COSF(ELB*R)
      SEB=SINF(ELB*R)
C      STORING TABLE FOR FOURIER TRANSFORM
      DO 78 I=1,400
   78 CT(I)=COSF(2.*3.141592653*(I-1)/400.)
C     WK IS WEIGHTING FUNCTION FOR AUTOCORRELATION FUNCTIONS
      DO 17 K=1,100
   17 WK(K)=.5+.5*COSF((3.14159*(K-1))/100.)
  900 INUM=0
      WRITE(59,955)
  955 FORMAT(37HNEW OUTPUT TAPE REQUIRES JUMP SW 2 ON)
      PAUSE
      ISRCH=3
   99 CONTINUE
      GO TO (928,929) SSWTCHF(2)
  928 WRITE(59,930)
  930 FORMAT(14HMOUNT NEW TAPE)
      PAUSE
      GO TO (961,929) SSWTCHF(2)
  961 END FILE 20
      REWIND 20
  929 CONTINUE
      INUM=INUM+1
      DO 77 I=1,5
   77 TIME(I)=86400.
      DO 18 K=1,100
      Y(K)=0.
      U(K)=0.
   18 X(K)=0.
      IREP=0
      IMIS=0
      IT=0.
      PP=0.
      QQ=0.
      RR=0.
      GO TO (3,3,119,184) ISRCH
```

```
  184 ISRCH=2
      GO TO 119
C     READ INPUT PARAMETERS
  119 WRITE(59,120)
  120 FORMAT(28HTYPE T FOR CLIPPED TRANSFORM)
      READ(58,121) OT
  121 FORMAT(A1)
      WRITE(59,101)
  101 FORMAT(31H CENTER FREQUENCY IN MEGACYCLES)
      READ(58,102)PA
  102 FORMAT(80R1)
      CALL NUMBERS(PA,80,ANS,NA)
      IF(NA)103,104,103
  103 FREQ=ANS(NA)
  104 WRITE(59,105)
  105 FORMAT(47HINST PHASE IN DEGREES AND DELAY IN MICROSECONDS)
      READ(58,106)PA
  106 FORMAT(80R1)
      CALL NUMBERS(PA,80,ANS,NA)
      IF(NA)108,109,108
  108 PINST=ANS(NA-1)
      DELAY=ANS(NA)
  109 WRITE(59,110) FREQ,PINST,DELAY
  110 FORMAT(4HFREQ,F10.4,12HMC/S INST PH,F8.3,11H DEG  DELAY,F9.3,9H MI
     1CROSEC)
      WRITE(59,112)
  112 FORMAT(5HTITLE)
      READ (58,113) TIT
  113 FORMAT(14A4)
      IF(TIT ,EQ. 1H )123,124
  124 DO 125 I=1,21
  125 TITLE(I)=TIT(I)
  123 WRITE(59,114)
  114 FORMAT(6H HAPPY)
      READ(58,115) REPLY
  115 FORMAT(A2)
      IF(REPLY.EQ. 2HNO) 119,116
  116 CONTINUE
      WC=FREQ*12.*2.54000508/29979.29
      W=WC*DBAS
C
C      **********************************************************************
C
    3 CALL INFREAD(F,T,ASUM,SC,PAR,NH,MODE,NINT,NBW,ISUM,NC)
C     NC   -1   PARITY ERROR
C             0   END OF FILE
C             2   TITLE
C             1   GEORGE≠S PROGRAM
C             3   PARTIAL SYSTEMS RECORDING
C             5   CHANNEL 5
C             6   CHANNEL 6 (AUTOCORRELATION FUNCTIONS)
      NC=NC+2
      GO TO (100,300,200,400,500,600,700,800,600) NC
  600 GO TO 3
  400 CALL ICVT(2,19,KI,-1)
      KI(1)=KI(1)-1900
      DO 401 I=1,28
  401 NHT(I)=NH(I)
      GO TO 3
```

```
  100 WRITE(59,199)
  199 FORMAT(23H PARITY ERROR, PRESS GO)
      PAUSE
      GO TO 3
  500 GO TO (3,534,529) ISRCH
  529 NHOUR=PAR(3)/3600.
      NMIN=(PAR(3)-NHOUR*3600.)/60.
      NSEC=PAR(3)-NHOUR*3600.-NMIN*60.
      WRITE(59,530) NHOUR,NMIN,NSEC
  530 FORMAT(I4,6H HOURS,I4,4H MIN,I4,4H SEC)
      WRITE(59,531)
  531 FORMAT(33H TYPE 1 SKIP, 2 PROCESS, 3 REINIT)
      READ (58,532) ISRCH
  532 FORMAT(I1)
      GO TO (3,534,119) ISRCH
  534 DO 501 L=1,5
      M=6-L
      AZS(M+1)=AZS(M)
      TIME(M+1)=TIME(M)
      ELS(M+1)=ELS(M)
  501 PH(M+1)=PH(M)
C     SOURCE COORD
      AZS(1)=PAR(1)
      ELS(1)=PAR(2)+PAR(4)
      TIME(1)=PAR(3)
      CES=COSF(ELS(1))
      SES=SINF(ELS(1))
C      COMPUTE REFERENCE PHASE  PH(I)
      PH(1)=2.*3.141592653*WC*(DBAS*(SEB*SES+CEB*CES*COSF(AZS(1)-AZB*R))
     1 -DMIL*CES/12.)
      PASC=PAR(5)
      DECL=PAR(6)
      GO TO 3
  700 IF(MODE)3,701,3
  701 BW=N8W
      BW=BW/1000.
      GO TO (702,3) SSWTCHF(5)
  702 ISRCH=4
      GO TO 99
C
C     ***************************************************************************
C
  800 GO TO (3,880,3)ISRCH
  880 IF(MODE)3,809,3
  809 DO 802 I=2,6
      IF(PAR(1)-86384.)803,3,3
  803 IF(PAR(1)-TIME(I))802,802,818
  802 CONTINUE
      GO TO 3
  818 DO 816 J=1,4
      IDIF=(PAR(J+1)-PAR(J))*40.+.5
      IF(IDIF-8) 817,816,817
  817 IMIS=IMIS+1
  816 CONTINUE
      DO 815 J=1,5
      IF(ISUM(1,1,J))811,3  ,811
C     COMPUTE REF PHASE AT TIME DATA IS TAKEN
  811 PHREF(J)=PH(I)+(PH(I-1)-PH(I))*(PAR(J)-TIME(I))/(TIME(I-1)-TIME(I)
     1)
```

```
      SPR(J)=SINF(PHREF(J))
      CPR(J)=COSF(PHREF(J))
      PP=PP+CPR(J)**2
      QQ=QQ+SPR(J)**2
      RR=RR+CPR(J)*SPR(J)
  815 CONTINUE
      IT=IT+1
      IF(IT-1)806,807,806
  807 P1=PHREF(1)
      T1=PAR(1)
      IH1=PAR(1)/3600.
      IM1=(PAR(1)-IH1*3600)/60.
      IS1=PAR(1)-IH1*3600-IM1*60
      XINT=(PAR(1)-TIME(I))/(TIME(I-1)-TIME(I))
      A1=(AZS(I)+(AZS(I-1)-AZS(I))*XINT)/R
      E1=(ELS(I)+(ELS(I-1)-ELS(I))*XINT)/R
C     SUM PRODUCTS OD AC FUNCS AND  COSINE AND SINE OF PHASE
  806 IF(OT .EQ. 1HT) 840,841
  840 DO 842 J=1,5
      DO 842 K=1,100
  842 U(K)=0.
  841 DO 808 J=1,5
      CP(J)=CPR(J)*PIE/ISUM(1,1,J)
      SP(J)=SPR(J)*PIE/ISUM(1,1,J)
      DO 808 K=1,100
      DX=ISUM(1,K,J)-ISUM(2,K,J)
      X(K)=X(K)+DX*CP(J)
  808 Y(K)=Y(K)+DX*SP(J)
      T2=PAR(5)
      A2=(AZS(I)+(AZS(I-1)-AZS(I))*(PAR(5)-TIME(I))/(TIME(I-1)-TIME(I)))
     1/R
      E2=(ELS(I)+(ELS(I-1)-ELS(I))*(PAR(5)-TIME(5))/(TIME(I-1)-TIME(I)))
     1/R
      GO TO 3
C
C      **********************************************************************
C
  300 WRITE(59,301)
  301 FORMAT(11HEND OF TAPE)
      REWIND 30
      PAUSE
      GO TO 900
  200 GO TO (279,204,279)ISRCH
  279 ISRCH=3
      GO TO 3
  204 P2=PHREF(5)
      IH2=T2/3600.
      IM2=(T2-IH2*3600.)/60.
      IS2=T2-IH2*3600-IM2*60
C     LOCAL HOUR ANGLE
      MH=PAR(5)/3600.
      MM=(PAR(5)-MH*3600.)/60.
      MS=PAR(5)-MH*3600.-MM*60.
      AZIM=(A2+A1)/2.
      ELEV=(E2+E1)/2.
      FR=(P2-P1)/(2.*3.1415926)
      DO 209 I=1,100
      U(I)=U(I)/(IT*5.)
      X(I)=X(I)/(IT*5.)
  209 Y(I)=Y(I)/(IT*5.)
```

```
C       COMPUTE FOURIER TRANSFORM
        DO 203 I=1,200
        XT(I)=0.
        YT(I)=0.
        TRANS(I)=0.
        DO 203 K=2,100
        N=(I-1)*(K-1)-(((I-1)*(K-1)/400)*400+1
        TRANS(I)= 2.*U(K)*WK(K)*CT(N)+TRANS(I)
        XT(I)=2.*X(K)*WK(K)*CT(N)+XT(I)
  203   YT(I)=2.*Y(K)*WK(K)*CT(N)+YT(I)
        DO 205 I=1,200
        XNUM=RR*XT(I)-PP*YT(I)
        XDEN=QQ*XT(I)-RR*YT(I)
        CALL ARCT(XNUM,XDEN,PHA(I))
        TAU=(P2+P1)/(2.*FREQ)+DELAY*2.*3.14159
C       SUBTRACT INSTRUMENTAL PHASE WHICH IS FREQ DEP
        PHASE(I)=PHA(I)-PINST*R-(I-101)*TAU*BW/160.
        IF(PHASE(I))220,222,221
  221   NUMB=(PHASE(I)+3.141592653)/(2.*3.141592653)
        GO TO 223
  220   NUMB=(PHASE(I)-3.141592653)/(2.*3.141592653)
  223   PHASE(I)=PHASE(I)/R-NUMB*360.
  222   IF(PHA(I))224,205,225
  225   NUMB=(PHA(I)+3.141592653)/(2.*3.141592653)
        GO TO 227
  224   NUMB=(PHA(I)-3.141592653)/(2.*3.141592653)
  227   PHA(I)=PHA(I)/R-NUMB*360.
  205   AMP(I)=SQRTF((YT(I)**2)*(RR**2+PP**2)*(XT(I)**2)*(QQ**2+RR**2)-
     1  2.*XT(I)*YT(I)*RR*(PP*QQ))*(IT*5.)/(PP*QQ-R**2)
C         AVERAGE PHASE AND AMPLITUDE FOR CONTINUUM SOURCES
        YC=0.
        XC=0.
        YS=0.
        XS=0.
        DO 207 I=21,181
        YC=YC+YT(I)*COSF((I-101)*TAU*BW/160.)
        YS=YS+YT(I)*SINF((I-101)*TAU*BW/160.)
        XC=XC+XT(I)*COSF((I-101)*TAU*BW/160.)
  207   XS=XS+XT(I)*SINF((I-101)*TAU*BW/160.)
        XNUM=-YC-XS
        XDEN=XC-YS
        CALL ARCT(XNUM,XDEN,PCAL)
        PCAL=PCAL/R-PINST
        PAMP=SQRTF(QQ*QQ*(YC+XC)**2+PP*PP*(XC-YS)**2)*IT*5./(PP*QQ*161.)
C
C       ***************************************************************
C
C       LIST ALL POWER SPECTRA  ETC
        PRINT 286,( NHT(I),I=1,27)
  286   FORMAT(1H1,3X,27A4,/)
        PRINT 949,(PNH(I),I=1,405)
  949   FORMAT(1X,135R1,/,1X,135R1,/,1X,135R1,/)
        GO TO (252,254) SSWTCHF(3)
  254   PRINT 287
  287   FORMAT(10X,6HFREQUENCY     COSINE AUTOCORR     SINE AUTOCORR
     1  SUM AUTOCORR///)
        PRINT 289,(I,X(I),Y(I),U(I),I=1,100)
  289   FORMAT(10X,I4,3F20.7)
        PRINT 291
```

```
     2 IMIS,MH,MM,MS,DECL
  270 FORMAT(21A4,19HBASELINE PARAMETERS,37X,6HLENGTH,F10,2,6H  FEET,34X
     1,F16.2,12H  WAVELENGTH,28X,9HELEVATION,F9,4,8H DEGREES,30X,
     27HAZIMUTH,F11.4,8H DEGREES,86X,5HDELAY,F18.3,5H MICS,28X,
     310HINST PHASE,F13.3,4H DEG,29X,9HFREQUENCY,F14.4,5H MC/S,28X,
     410HTIME START,3I4,  34X,10HAZ   START,F13,3,33X,10HEL   START,
     5F13.3,33X,10HPH   START,F13.3,33X,10HTIME  STOP,3I4,  34X,
     610HAZ    STOP,F13.3,33X,10HEL    STOP,F13,3,33X,10HPH    STOP,
     7F13.3,33X,10HFRINGES   ,F13,3,33X,10HINT TIME  ,I10  ,8H  CYCLES,
     856X,5HDATE ,5X,3I4,34X,9HBANDWIDTH,F10.2,5H MC/S,32X,6HMISSES, 10,
     940X,10HLOCAL H.A.,3I4,34X,3HDEC,F12,4,4H DEG)
C      PLOT COSINE TRANSFORM
       GO TO(910,251) SSWTCHF(3)
  251  GO TO (901,262) SSWTCHF(1)
  901  IF(INUM-1)233,262,233
  262  WRITE (59, 230)                                                  COS
  230  FORMAT(29H SET FOURIER TRANSFORM LIMITS)
       READ(58,102)PA
       CALL NUMBERS(PA,80,ANS,NA)
       IF(NA)232,233,232
  232  XTMAX=ANS(NA-1)
       XTMIN=ANS(NA)
  291  FORMAT(1H1,106H FREQUENCY  COS TRANSFORM  SIN TRANSFORM      RAW P
     1HASE     FRINGE AMPLITUDE  FRINGE PHASE   SUM TRANSFORM//)
       PRINT 290,(I,XT(I),YT(I),PHA(I),AMP(I),PHASE(I),TRANS(I),I=1,200)
  290  FORMAT( 5X,I4,6F16,4)
       GO TO 292
  252  PRINT 293
  293  FORMAT(20X, 93HNUMBER    FRINGE AMP   PHASE    NUMBER    FRINGE AM
     1P    PHASE    NUMBER    FRINGE AMP   PHASE/)
       DO 294 I=1,53
       J=I+20
       K=I+73
       L=I+127
       PRINT 253,J,AMP(J),PHASE(J),K,AMP(K),PHASE(K),L,AMP(L),PHASE(L)
  253  FORMAT(14X,I12,F11,4,F10.1,I12,F11.4,F10.1,I12,F11.4,F10.1)
  294  CONTINUE
C      OUTPUT TAPE     WILL SPACE TO END OF FILE MARK                   OUTPUT
  292  CALL SEFF(20)
       BACKSPACE 20
       WRITE (20) U,X,Y,XT,YT,TRANS,PHA,PHASE,AMP,KI,T1,T2,A2,A1,E2,E1,
     1 FR,IT,PCAL,AZB,ELB,DBAS,FREQ,W,F,T,ASUM,SC,PAR,NH,BW,PINST,
     2 TITLE,P1,P2,RASC,DECL
       END FILE 20
       BACKSPACE 20
       PRINT 984
  984  FORMAT(////)
       PRINT 211,AZIM,ELEV,PCAL,PAMP
  211  FORMAT(10X,12HMEAN AZIMUTH,F10.4,//10X,14HMEAN ELEVATION,F8.4//,
     1 10X,12HFRINGE PHASE,F10.4//,10X,16HFRINGE AMPLITUDE,F12.4)
C
C      ***************************************************************
C
C      ENCODE VARIABLES WHICH APPEAR ON GRAPHS
       ENCODE(24,268,LABELX)
  268  FORMAT(10X,14HCHANNEL NUMBER)
       BW=ABSF(BW)
       ENCODE(1456,270,INFO)TITLE,DBAS,W,ELB,AZB,DELAY,PINST,FREQ,IH1,
     1IM1,IS1,A1,E1,P1,IH2,IM2,IS2,A2,E2,P2,FR,IT,KI(2),KI(3),KI(1),BW,
```

```
  265 CALL LIMITS(1.,101.,-180.,180.)
      DO 245 I=2,200,2
      XX=I/2
      YY=PHASE(I)
  245 CALL POINTS(XX,YY,1R*,1)
      CALL GRIDS(1.,10.,180.,-60.)
      ENCODE(16,285,LABELY)
  285 FORMAT(4X,12HFRINGE PHASE)
       CALL LABELS(LABELX,6,LABELY,4)
      CALL GRAPHS(INFO,15,364,1)
      IF(IREP)906,267,906
  267 IF(OT .EQ. 1H )299,272
  272 WRITE (59, 273)
  233 CALL LIMITS(1.,101.,XTMIN,XTMAX)
      DO 242 I=2,200,2
      XX=I/2
      YY=XT(I)
  242 CALL POINTS(XX,YY,1R*,1)
      CALL GRIDS(1.,10.,XTMAX,-(XTMAX-XTMIN)/4.)
      ENCODE(16,269,LABELY)
  269 FORMAT(16HCOSINE TRANSFORM)
       CALL LABELS(LABELX,6,LABELY,4)
      CALL GRAPHS(INFO,15,364,1)
C     PLOT SINE TRANSFORM
      CALL LIMITS(1.,101.,XTMIN,XTMAX)                                  SIN
      DO 243 I=2,200,2
      XX=I/2
      YY=YT(I)
  243 CALL POINTS(XX,YY,1R*,1)
      CALL GRIDS(1.,10.,XTMAX,-(XTMAX-XTMIN)/4.)
      ENCODE(14,280,LABELY)
  280 FORMAT(14HSINE TRANSFORM)
       CALL LABELS(LABELX,6,LABELY,4)
      CALL GRAPHS(INFO,15,364,1)
      IF(IREP)906,910,906
C     PLOT FRINGE AMPLITUDE
  910 GO TO (902,264) SSWTCHF(1)
  902 IF(INUM-1)237,264,237
  264 WRITE (59, 235)                                                   AMP
  235 FORMAT(28H SET FRINGE AMPLITUDE LIMITS)
      READ(58,102)PA
      CALL NUMBERS(PA,80,ANS,NA)
      IF(NA)236,237,236
  236 AMAX=ANS(NA-1)
      AMIN=ANS(NA)
  237 CALL LIMITS(1.,101.,AMIN,AMAX)
      DO 244 I=2,200,2
      XX=I/2
      YY=AMP(I)
  244 CALL POINTS(XX,YY,1R*,1)
      CALL GRIDS(1.,10.,AMAX,-(AMAX-AMIN)/4.)
      ENCODE(16,282,LABELY)
  282 FORMAT(16HFRINGE AMPLITUDE)
       CALL LABELS(LABELX,6,LABELY,4)
      CALL GRAPHS(INFO,15,364,1)
      IF(IREP)299,265,299
C     PLOT FRINGE PHASE
```

```
  273 FORMAT(25H SET POWER SPECTRA LIMITS)
      READ(58,102)PA
      CALL NUMBERS(PA,80,ANS,NA)
      IF(NA)274,275,274
  274 TMAX=ANS(NA-1)
      TMIN=ANS(NA)
  275 CALL LIMITS(1.,101.,TMIN,TMAX)
      DO 276 I=2,200,2
      XX=I/2
      YY=TRANS(I)
  276 CALL POINTS(XX,YY,1R*,1)
      CALL GRIDS(1.,10.,TMIN,-(TMAX-TMIN)/4,)
      ENCODE(13,277,LABELY)
  277 FORMAT(13HPOWER SPECTRA)
       CALL LABELS(LABELX,6,LABELY,4)
      CALL GRAPHS(INFO,15,364,1)
  299 GO TO (905,906) SSWTCHF(1)
  905 ISRCH=2
      GO TO 99
C     IREP=0,NO REPLOT,1 COS AND SIN TRANS, 2 COS AND SIN TRANS,
C     3 FRINGE AMPLITUDE 4 SUM TRANSFORM
  906 WRITE (59, 295)
  295 FORMAT(12H REPLOT 1=4 )
      READ(58,296) IREP
  296 FORMAT(I1)
      IREP=IREP+1
      GO TO(261,262,262,264,267) IREP
  261 CONTINUE
      WRITE (59, 969)
  969 FORMAT( 41H JUMP SWITCH 1 ON FOR NON STOP PROCESSING)
      PAUSE
      GO TO (905,970) SSWTCHF(1)
  970 WRITE (59, 278)
  278 FORMAT(63HTYPE  1 SKIP, 2 PROCESS, 3 REINT AND SKIP, 4 REINT AND
     1PROCESS)
      READ(58,297) ISRCH
  297 FORMAT(I1)
      GO TO 99
      END

        3200 FORTRAN DIAGNOSTIC RESULTS - FOR   MILSTAK

ERRORS
```

Acknowledgment

The author is grateful to a large number of people who contributed to this work. J. M. Moran, Patricia P. Crowther, and J. A. Ball wrote the computer programs. G. M. Hyde, V. C. Pineo, and J. C. Carter provided engineering assistance. R. H. Erickson, R. Lewis, and D. C. Papa constructed much of the equipment. The author is particularly indebted to Professor Bernard F. Burke who initiated the project and provided much of the theoretical and practical knowledge. Finally, the author is indebted to Professor Alan H. Barrett for supervising this work as a portion of thesis research that is being undertaken at the Massachusetts Institute of Technology.

References

1. S. Weinreb, "A Digital Spectral Analysis Technique and Its Application to Radio Astronomy," Technical Report 412, Research Laboratory of Electronics, Massachusetts Institute of Technology, Cambridge, Mass., August 30, 1963.
2. J. H. Van Vleck, Report No. 51, Radio Research Laboratory, Harvard University, Cambridge, Mass., July 21, 1943.
3. F. E. Heart, A. A. Mathiasen, and P. D. Smith, "The Haystack Computer Control System," Technical Report 406, Lincoln Laboratory, Massachusetts Institute of Technology, Lexington, Mass., 27 October 1965.
4. G. H. Conant, "Radiometric Spectral-Line Processing in the Haystack Antenna Pointing System" (in preparation for publication).

JOINT SERVICES ELECTRONICS PROGRAM
REPORTS DISTRIBUTION LIST

Department of Defense

Dr. Edward M. Reilley
Asst Director (Research)
Ofc of Defense Res & Eng
Department of Defense
Washington, D.C. 20301

Office of Deputy Director
(Research and Information Room 3D1037)
Department of Defense
The Pentagon
Washington, D.C. 20301

Director
Advanced Research Projects Agency
Department of Defense
Washington, D.C. 20301

Director for Materials Sciences
Advanced Research Projects Agency
Department of Defense
Washington, D.C. 20301

Headquarters
Defense Communications Agency (333)
The Pentagon
Washington, D.C. 20305

Defense Documentation Center
Attn: TISIA
Cameron Station, Bldg. 5
Alexandria, Virginia 22314

Director
National Security Agency
Attn: Librarian C-332
Fort George G. Meade, Maryland 20755

Weapons Systems Evaluation Group
Attn: Col. Daniel W. McElwee
Department of Defense
Washington, D.C. 20305

National Security Agency
Attn: R4-James Tippet
Office of Research
Fort George G. Meade, Maryland 20755

Central Intelligence Agency
Attn: OCR/DD Publications
Washington, D.C. 20505

Department of the Air Force

Colonel Kee
AFRSTE
Hqs. USAF
Room ID-429, The Pentagon
Washington, D.C. 20330

Colonel A. Swan
Aerospace Medical Division
Brooks Air Force Base, Texas 78235

AUL3T-9663
Maxwell AFB, Alabama 36112

AFFTC (FTBPP-2)
Technical Library
Edwards AFB, Calif. 93523

Space Systems Division
Air Force Systems Command
Los Angeles Air Force Station
Los Angeles, California 90045
Attn: SSSD

Major Charles Waespy
Technical Division
Deputy for Technology
Space Systems Division, AFSC
Los Angeles, California 90045

SSD(SSTRT/Lt. Starbuck)
AFUPO
Los Angeles, California 90045

Det #6, OAR (LOOAR)
Air Force Unit Post Office
Los Angeles, California 90045

Systems Engineering Group (RTD)
Technical Information Reference Branch
Attn: SEPIR
Directorate of Engineering Standards
and Technical Information
Wright-Patterson AFB, Ohio 45433

ARL (ARIY)
Wright-Patterson AFB, Ohio 45433

Dr. H. V. Noble
Air Force Avionics Laboratory
Wright-Patterson AFB, Ohio 45433

Mr. Peter Murray
Air Force Avionics Laboratory
Wright-Patterson AFB, Ohio 45433

AFAL (AVTE/R. D. Larson)
Wright-Patterson AFB, Ohio 45433

Commanding General
Attn: STEWS-WS-VT
White Sands Missile Range
New Mexico 88002

RADC (EMLAL-1)
Griffiss AFB, New York 13442
Attn: Documents Library

Academy Library (DFSLB)
U.S. Air Force Academy
Colorado Springs, Colorado 80912

Lt. Col. Bernard S. Morgan
Frank J. Seiler Research Laboratory
U.S. Air Force Academy
Colorado Springs, Colorado 80912

APGC (PGBPS-12)
Eglin AFB, Florida 32542

AFETR Technical Library
(ETV, MU-135)
Patrick AFB, Florida 32925

AFETR (ETLLG-1)
STINFO Officer (for Library)
Patrick AFB, Florida 32925

Dr. L. M. Hollingsworth
AFCRL (CRN)
L. G. Hanscom Field
Bedford, Massachusetts 01731

AFCRL (CRMXLR)
AFCRL Research Library, Stop 29
L. G. Hanscom Field
Bedford, Massachusetts 01731

Colonel Robert E. Fontana
Department of Electrical Engineering
Air Force Institute of Technology
Wright-Patterson AFB, Ohio 45433

Colonel A. D. Blue
RTD (RTTL)
Bolling Air Force Base, D.C. 20332

Dr. I. R. Mirman
AFSC (SCT)
Andrews Air Force Base, Maryland 20331

Colonel J. D. Warthman
AFSC (SCTR)
Andrews Air Force Base, Maryland 20331

Lt. Col. J. L. Reeves
AFSC (SCBB)
Andrews Air Force Base, Maryland 20331

ESD (ESTI)
L. G. Hanscom Field
Bedford, Massachusetts 01731

AEDC (ARO, INC)
Attn: Library/Documents
Arnold AFS, Tennessee 37389

European Office of Aerospace Research
Shell Building
47 Rue Cantersteen
Brussels, Belgium

Lt. Col. Robert B. Kalisch
Chief, Electronics Division
Directorate of Engineering Sciences
Air Force Office of Scientific Research
Arlington, Virginia 22209

Department of the Army

U.S. Army Research Office
Attn: Physical Sciences Division
3045 Columbia Pike
Arlington, Virginia 22204

Research Plans Office
U.S. Army Research Office
3045 Columbia Pike
Arlington, Virginia 22204

Commanding General
U.S. Army Materiel Command
Attn: AMCRD-RS-DE-E
Washington, D.C. 20315

Commanding General
U.S. Army Strategic Communications
Command
Washington, D.C. 20315

Commanding Officer
U.S. Army Materials Research Agency
Watertown Arsenal
Watertown, Massachusetts 02172

Commanding Officer
U.S. Army Ballistics Research Laboratory
Attn: V. W. Richards
Aberdeen Proving Ground
Aberdeen, Maryland 21005

Commandant
U.S. Army Air Defense School
Attn: Missile Sciences Division C&S Dept.
P.O. Box 9390
Fort Bliss, Texas 79916

Commanding General
U.S. Army Missile Command
Attn: Technical Library
Redstone Arsenal, Alabama 35809

Commanding General
Frankford Arsenal
Attn: L600-64-4 (Dr. Sidney Ross)
Philadelphia, Pennsylvania 19137

U.S. Army Munitions Command
Attn: Technical Information Branch
Picatinney Arsenal
Dover, New Jersey 07801

Commanding Officer
Harry Diamond Laboratories
Attn: Dr. Berthold Altman (AMXDO-TI)
Connecticut Avenue and Van Ness St. N. W.
Washington, D.C. 20438

Commanding Officer
U.S. Army Security Agency
Arlington Hall
Arlington, Virginia 22212

Commanding Officer
U.S. Army Limited War Laboratory
Attn: Technical Director
Aberdeen Proving Ground
Aberdeen, Maryland 21005

Commanding Officer
Human Engineering Laboratories
Aberdeen Proving Ground, Maryland 21005

Director
U.S. Army Engineer
Geodesy, Intelligence and Mapping
Research and Development Agency
Fort Belvoir, Virginia 22060

Commandant
U.S. Army Command and General
Staff College
Attn: Secretary
Fort Leavenworth, Kansas 66270

Dr. H. Robl, Deputy Chief Scientist
U.S. Army Research Office (Durham)
Box CM, Duke Station
Durham, North Carolina 27706

Commanding Officer
U.S. Army Research Office (Durham)
Attn: CRD-AA-IP (Richard O. Ulsh)
Box CM, Duke Station
Durham, North Carolina 27706

Librarian
U.S. Army Military Academy
West Point, New York 10996

The Walter Reed Institute of Research
Walter Reed Medical Center
Washington, D.C. 20012

Commanding Officer
U.S. Army Engineer R&D Laboratory
Attn: STINFO Branch
Fort Belvoir, Virginia 22060

Commanding Officer
U.S. Army Electronics R&D Activity
White Sands Missile Range,
New Mexico 88002

Dr. S. Benedict Levin, Director
Institute for Exploratory Research
U.S. Army Electronics Command
Fort Monmouth, New Jersey 07703

Director
Institute for Exploratory Research
U.S. Army Electronics Command
Attn: Mr. Robert O. Parker, Executive
Secretary, JSTAC (AMSEL-XL-D)
Fort Monmouth, New Jersey 07703

Commanding General
U.S. Army Electronics Command
Fort Monmouth, New Jersey 07703
Attn: AMSEL-SC
RD-D
RD-G
RD-GF
RD-MAT
XL-D
XL-E
XL-C
XL-S
HL-D
HL-CT-R
HL-CT-P
HL-CT-L
HL-CT-O
HL-CT-I
HL-CT-A
NL-D
NL-A
NL-P
NL-R
NL-S
KL-D
KL-E
KL-S
KL-TM
KL-TQ
KL-TS
VL-D
WL-D

Department of the Navy

Chief of Naval Research
Department of the Navy
Washington, D.C. 20360
Attn: Code 427

Naval Electronics Systems Command
ELEX 03
Falls Church, Virginia 22046

Naval Ship Systems Command
SHIP 031
Washington, D.C. 20360

Naval Ship Systems Command
SHIP 035
Washington, D.C. 20360

Naval Ordnance Systems Command
ORD 32
Washington, D.C. 20360

Naval Air Systems Command
AIR 03
Washington, D.C. 20360

Commanding Officer
Office of Naval Research Branch Office
Box 39, Navy No 100 F.P.O.
New York, New York 09510

Commanding Officer
Office of Naval Research Branch Office
219 South Dearborn Street
Chicago, Illinois 60604

Commanding Officer
Office of Naval Reasearch Branch Office
1030 East Green Street
Pasadena, California 91101

Commanding Officer
Office of Naval Research Branch Office
207 West 24th Street
New York, New York 10011

Commanding Officer
Office of Naval Research Branch Office
495 Summer Street
Boston, Massachusetts 02210

Director, Naval Research Laboratory
Technical Information Officer
Washington, D.C. 20360
Attn: Code 2000

Commander
Naval Air Development and Material Center
Johnsville, Pennsylvania 18974

Librarian
U.S. Naval Electronics Laboratory
San Diego, California 95152

Commanding Officer and Director
U.S. Naval Underwater Sound Laboratory
Fort Trumbull
New London, Connecticut 06840

Librarian
U.S. Navy Post Graduate School
Monterey, California 93940

Commander
U.S. Naval Air Missile Test Center
Point Magu, California 93041

Director
U.S. Naval Observatory
Washington, D.C. 20390

Chief of Naval Operations
OP-07
Washington, D.C. 20350

Director, U.S. Naval Security Group
Attn: G43
3801 Nebraska Avenue
Washington, D.C. 20390

Commanding Officer
Naval Ordnance Laboratory
White Oak, Maryland 21502

Commanding Officer
Naval Ordnance Laboratory
Corona, California 91720

Commanding Officer
Naval Ordnance Test Station
China Lake, California 93555

Commanding Officer
Naval Avionics Facility
Indianapolis, Indiana 46241

Commanding Officer
Naval Training Device Center
Orlando, Florida 32811

U.S. Naval Weapons Laboratory
Dahlgren, Virginia 22448

Gordon McKay Library A175
Technical Reports Collection
Harvard College
Cambridge, Massachusetts 02138

Aerospace Corporation
P.O. Box 95085
Los Angeles, California 90045
Attn: Library Acquisitions Group

Professor Nicholas George
California Institute of Technology
Pasadena, California 91109

Aeronautics Library
Graduate Aeronautical Laboratories
California Institute of Technology
1201 E. California Blvd.
Pasadena, California 91109

Director, USAF Project RAND
Via: Air Force Liaison Office
The RAND Corporation
1700 Main Street
Santa Monica, California 90406
Attn: Library

The Johns Hopkins University
Applied Physics Laboratory
8621 Georgia Avenue
Silver Spring, Maryland 20910
Attn: Boris W. Kuvshinoff
Document Librarian

Hunt Library
Carnegie Institute of Technology
Schenley Park
Pittsburgh, Pennsylvania 15213

Dr. Leo Young
Stanford Research Institute
Menlo Park, California 94025

Mr. Henry L. Bachmann
Assistant Chief Engineer
Wheeler Laboratories
122 Cuttermill Road
Great Neck, New York 11021

School of Engineering Sciences
Arizona State University
Tempe, Arizona 85281

Engineering and Mathematical
Sciences Library
University of California
405 Hilgrad Avenue
Los Angeles, California 90024

California Institute of Technology
Pasadena, California 91109
Attn: Documents Library

University of California
Santa Barbara, California 93106
Attn: Library

Carnegie Institute of Technology
Electrical Engineering Department
Pittsburgh, Pennsylvania 15213

University of Michigan
Electrical Engineering Department
Ann Arbor, Michigan 48104

New York University
College of Engineering
New York, New York 10019

Syracuse University
Dept. of Electrical Engineering
Syracuse, New York 13210

Yale University
Engineering Department
New Haven, Connecticut 06520

Airborne Instruments Laboratory
Deerpark, New York 11729

Bendix Pacific Division
11600 Sherman Way
North Hollywood, California 91605

General Electric Company
Research Laboratories
Schenectady, New York 12301

Lockheed Aircraft Corporation
P.O. Box 504
Sunnyvale, California 94088

Raytheon Company
Bedford, Massachusetts 01730
Attn: Librarian

Dr. G. J. Murphy
The Technological Institute
Northwestern University
Evanston, Illinois 60201

Dr. John C. Hancock, Director
Electronic Systems Research Laboratory
Purdue University
Lafayette, Indiana 47907

Weapons Systems Test Division
Naval Air Test Center
Patuxtent River, Maryland 20670
Attn: Library

Head, Technical Division
U.S. Naval Counter Intelligence
Support Center
Fairmont Building
4420 North Fairfax Drive
Arlington, Virginia 22203

Other Government Agencies

Mr. Charles F. Yost
Special Assistant to the Director
of Research
National Aeronautics and
Space Administration
Washington, D.C. 20546

Dr. H. Harrison, Code RRE
Chief, Electrophysics Branch
National Aeronautics and
Space Administration
Washington, D.C. 20546

Goddard Space Flight Center
National Aeronautics and
Space Administration
Attn: Library C3/TDL
Green Belt, Maryland 20771

NASA Lewis Research Center
Attn: Library
21000 Brookpark Road
Cleveland, Ohio 44135

National Science Foundation
Attn: Dr. John R. Lehmann
Division of Engineering
1800 G Street, N.W.
Washington, D.C. 20550

U.S. Atomic Energy Commission
Division of Technical Information Extension
P.O. Box 62
Oak Ridge, Tennessee 37831

Los Alamos Scientific Laboratory
Attn: Reports Library
P.O. Box 1663
Los Alamos, New Mexico 87544

NASA Scientific & Technical Information
Facility
Attn: Acquisitions Branch (S/AK/DL)
P.O. Box 33,
College Park, Maryland 20740

NASA, Langley Research Center
Langley Station
Hampton, Virginia 23365
Attn: Mr. R. V. Hess, Mail Stop 160

Non-Government Agencies

Director
Research Laboratory of Electronics
Massachusetts Institute of Technology
Cambridge, Massachusetts 02139

Polytechnic Institute of Brooklyn
55 Johnson Street
Brooklyn, New York 11201
Attn: Mr. Jerome Fox
Research Coordinator

Director
Columbia Radiation Laboratory
Columbia University
538 West 120th Street
New York, New York 10027

Director
Coordinated Science Laboratory
University of Illinois
Urbana, Illinois 61803

Director
Stanford Electronics Laboratories
Stanford University
Stanford, California 94305

Director
Electronics Research Laboratory
University of California
Berkeley, California 94720

Director
Electronic Sciences Laboratory
University of Southern California
Los Angeles, California 90007

Professor A. A. Dougal, Director
Laboratories for Electronics and
Related Sciences Research
University of Texas
Austin, Texas 78712

Director
Microwave Laboratory
Stanford University
Stanford, California 94305

Emil Schafer Head
Electronics Properties Info Center
Hughes Aircraft Company
Culver City, California 90230

UNCLASSIFIED
Security Classification

3ND PPSO 13152

DOCUMENT CONTROL DATA - R&D

(Security classification of title, body of abstract and indexing annotation must be entered when the overall report is classified)

1. ORIGINATING ACTIVITY *(Corporate author)* Research Laboratory of Electronics Massachusetts Institute of Technology Cambridge, Massachusetts	2a. REPORT SECURITY CLASSIFICATION Unclassified 2b. GROUP None

3. REPORT TITLE

The Haystack-Millstone Interferometer System

4. DESCRIPTIVE NOTES *(Type of report and inclusive dates)*

Technical Report

5. AUTHOR(S) *(Last name, first name, initial)*

Rogers, Alan E. E.

6. REPORT DATE	7a. TOTAL NO. OF PAGES	7b. NO. OF REFS
March 15, 1967	60	4

8a. CONTRACT OR GRANT NO.	9a. ORIGINATOR'S REPORT NUMBER(S)
DA 28-043-AMC-02536(E) b. PROJECT NO. 200-14501-B31F NASA Grant NsG-419	Technical Report 457 9b. OTHER REPORT NO(S) *(Any other numbers that may be assigned this report)*

10. AVAILABILITY/LIMITATION NOTICES

Distribution of this report is unlimited.

11. SUPPLEMENTARY NOTES	12. SPONSORING MILITARY ACTIVITY
	Joint Services Electronics Program thru USAECOM, Fort Monmouth, N. J.

13. ABSTRACT

The Haystack 120-ft antenna and the Millstone 84-ft antenna have been coupled together to form a radiometric interferometer. At 18-cm wavelength, which was chosen for a study of galactic OH emission, the interferometer has a minimum fringe spacing of 54 seconds of arc.The interferometer synthesizes a beam approximately equivalent to that of a 2000-ft parabolic antenna and can measure positions to a small fraction of the fringe spacing. The interferometer uses a digital correlator to analyze the fringe amplitude and phase as a function of frequency. This enables mapping of spectral features. The design and construction are described, as well as the theory and method of data reduction. A noise analysis shows that the threshold level could be reduced by using more complex processing techniques. It is shown that for radiometric studies many of the capabilities of a very large antenna can be synthesized, with smaller antennas and complex data-processing equipment taking the place of mechanical structure.

DD FORM 1 JAN 64 1473 IIA 0101 807 6800

UNCLASSIFIED
Security Classification

14. KEY WORDS	LINK A		LINK B		LINK C	
	ROLE	WT	ROLE	WT	ROLE	WT
Radiometric interferometer						
Haystack						
Millstone						
Noise analysis						
Digital correlator						
Spectial line interferometer						
aperture synthesis						
Radio Astronomy						
Servo-controlled transmission line						
Microwave interferometer						